Fluorogenic Probe Using a Mislow-Evans Rearrangement for Real-Time Imaging of Hydrogen Peroxide

Dianne Pham[1], Upamanyu Basu[1], Ivanna Pohorilets[1], Claudette M. St Croix[2], Simon C. Watkins[2], and Kazunori Koide[1]*

[1]Department of Chemistry, University of Pittsburgh, 219 Parkman Avenue, Pittsburgh, Pennsylvania 15260, United States

[2]Center for Biologic Imaging, Department of Cell Biology, University of Pittsburgh, 3500 Terrace Street, Pittsburgh, Pennsylvania 15261, United States

In memory of Professors Kurt Mislow and Hans J. Reich and dedicated to Professor David A. Evans

Abstract: Hydrogen peroxide (H_2O_2) mediates the biology of wound healing, apoptosis, inflammation, etc. H_2O_2 has been fluorometrically imaged with protein- or small molecule-based probes. However, only protein-based probes have afforded temporal insights within seconds. Small molecule-based electrophilic probes for H_2O_2 require many minutes for a sufficient response in biological systems. Here, we report a fluorogenic probe that selectively undergoes a [2,3]-sigmatropic rearrangement (seleno-Mislow-Evans rearrangement) with H_2O_2, followed by an acetal hydrolysis, to produce a green fluorescent molecule in seconds. Unlike other electrophilic probes, the current probe acts as a nucleophile. The fast kinetics enabled real-time imaging of H_2O_2 produced in endothelial cells in 8 seconds (much earlier than previously shown) and H_2O_2 in a zebrafish wound healing model. This work may provide a platform for endogenous H_2O_2 detection in real time with chemical probes.

Keywords: Fluorescent probe, Oxidation, Selenium, Peroxides, Sigmatropic rearrangement

Hydrogen peroxide (H_2O_2) is a reactive oxygen species (ROS) involved in many biological processes. As such, misregulation of H_2O_2 has been implicated in many diseases.[1] In the cell, H_2O_2 is produced along with other ROS in the mitochondria and cytoplasm by the NADPH oxidase family of enzymes, xanthine oxidase, and cytochrome P450 enzymes.[1a, 2] In light of the dichotomous nature of H_2O_2 in maintaining cellular homeostasis, it has become increasingly important to understand the detailed biology of H_2O_2.[1b, 3]

Only recently has the spatiotemporal presence of H_2O_2 in wound healing been recognized.[4] Additionally, ROS production is critical for defense against pathogens; however, early studies used nonselective probes for ROS and could not distinguish between effects caused specifically by H_2O_2.[3a, 5] Studies of biological H_2O_2 with high specificity and temporal resolution have relied on genetically encoded protein-based probes.[4a, 6] These studies using protein-based probes have revealed that upon injury to tissue, H_2O_2 is produced in seconds to minutes with gradients from the site of injury, facilitating the mobilization of immune cells.[4a] These results have not been observed using chemical probes, likely due to the comparatively slow reaction kinetics.

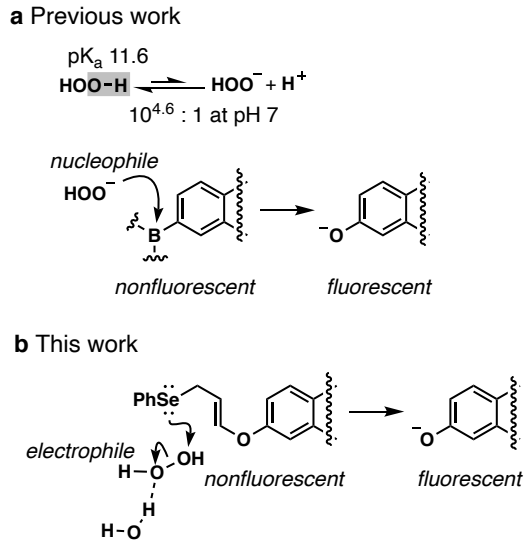

Figure 1. Comparison of (a) boronate-based and (b) selenium-based probes for hydrogen peroxide.

Most chemical probes for H_2O_2 have relied on the boronate ester functionality (Figure 1a) for reaction,[7] although other functionalities have been reported.[8] Advances from these studies have allowed for selective detection of H_2O_2 over other reactive oxygen and nitrogen species (RNS). This chemistry presumably requires the presence of the hydroperoxide anion, HOO^-. Under biological conditions, the abundance of this species should be very low (~0.1% of H_2O_2) because the pK_a of H_2O_2 is 11.6. When these probes were applied in biological systems, it took ca. 30 min to produce fluorescence signals.[7c, 7d, 7g, 8e]

To develop a new probe that more rapidly reacts intracellularly, in this study we used the seleno Mislow-Evans rearrangement, which undergoes the oxidation of an allylic selenide with H_2O_2 (Figure 1b).[9] This rearrangement is fast even at 0 °C[10] and requires the neutral and abundant form of H_2O_2 to act as an electrophile; this reactivity has not been exploited in the development of probes for H_2O_2. We hypothesized that the seleno Mislow-Evans rearrangement would provide a novel platform for the fluorometric detection of H_2O_2 with superior kinetics to more favorably compete with the degradation of H_2O_2 in cells. Here, we integrate the rearrangement with a spontaneous hydrolysis of the resulting acetal to translate the high reactivity of a selenium atom with H_2O_2 into a fluorogenic switch. We present the synthesis of selenide **1** and its selectivity for H_2O_2 over other ROS and RNS. We also show that selenide **1** can detect endogenously produced H_2O_2 by treatment with ionomycin in macrophages and in a zebrafish wound-healing experiment.

We envisioned that allylic selenide **1** (Figure 2A) could undergo oxidation with H_2O_2 through transition state **TS1**, followed by the Mislow-Evans rearrangement of selenoxide **2** and the subsequent hydrolysis of selenenate **3** to form the brightly fluorescent phenol **5**. For the conversion of **3** to **5**, two pathways are plausible. The first pathway is the nucleophilic cleavage of the Se-O bond of **3** to form hemiacetal **4**, which spontaneously forms phenoxide **5** and acrolein (Pathway 1). The second is the oxidation of selenenate **3** to seleninate **6** en route to phenol **5** via hemiacetal **4** (Pathway 2). As shown below, we experimentally determined the actual pathway.

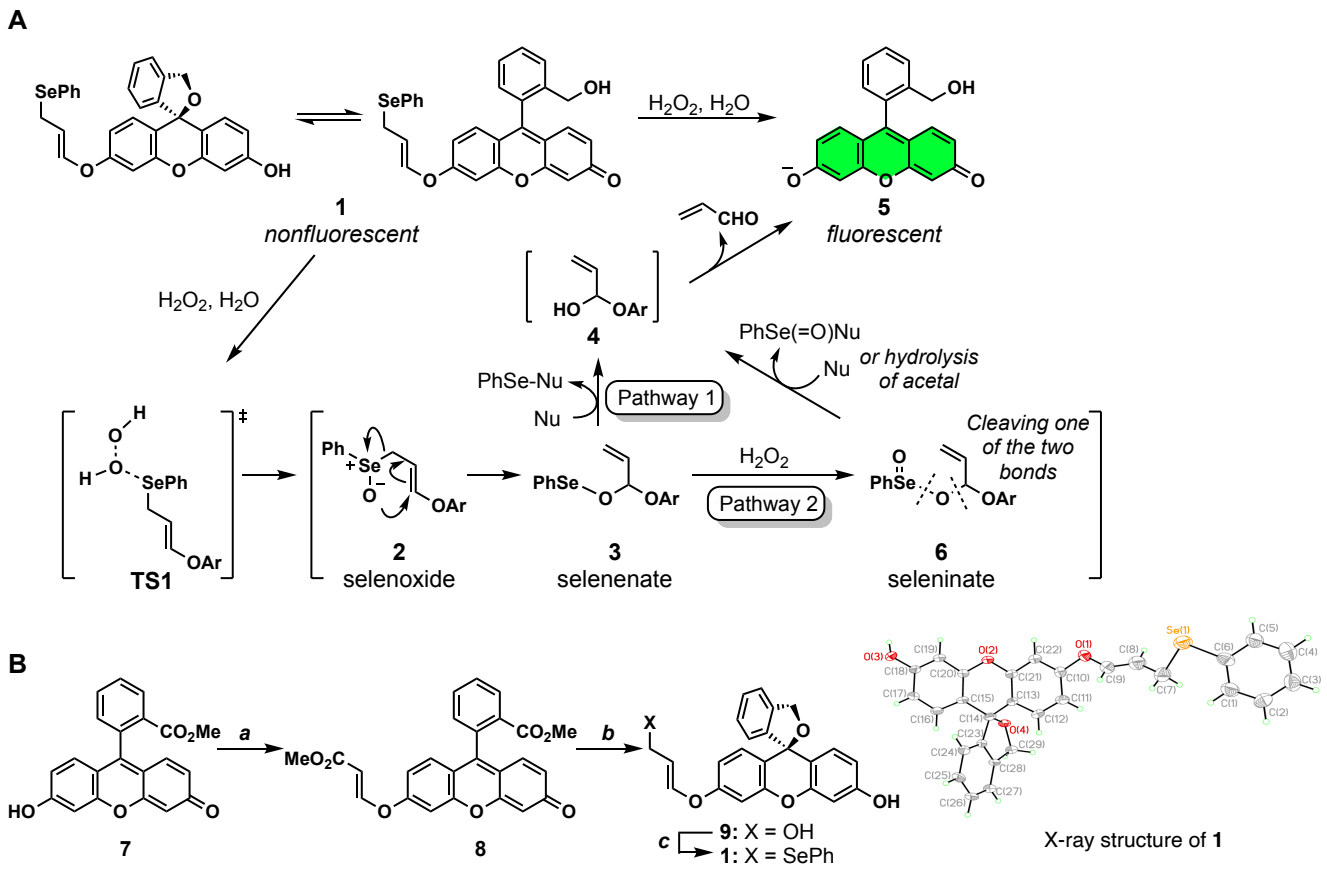

Figure 2. (A) Design of probe **1** based on the seleno-Mislow-Evans rearrangement followed by hydrolysis via two possible pathways. (B) Synthesis of probe **1**. Conditions: (a) *N*-Methylmorpholine (0.3 equiv), methyl propiolate (5.0 equiv), CH_2Cl_2, 24 h, 79 %; (b) DIBALH (7.8 equiv), CH_2Cl_2, -78 to 23 °C, 2 h; then DDQ (1.1 equiv), Et_2O, 3 h, 0 °C, 66 %; (c) $^nBu_3P$ (1.2 equiv), PhSeCN (1.0 equiv), THF, 0 °C, 30 min, 41 %.

The synthesis of selenide **1** (Figure 2B) commenced with the conjugate addition of fluorescein methyl ester **7** to methyl propiolate to afford ester **8** in 79% yield. The following DIBALH reduction formed alcohol **9** in 66% yield. The moderate yield was caused by the hydrolysis of the enol ether during aqueous workup. The final Mitsunobu-type reaction[11] afforded selenide **1** in 41% yield. The structure was confirmed by the X-ray structure analysis.

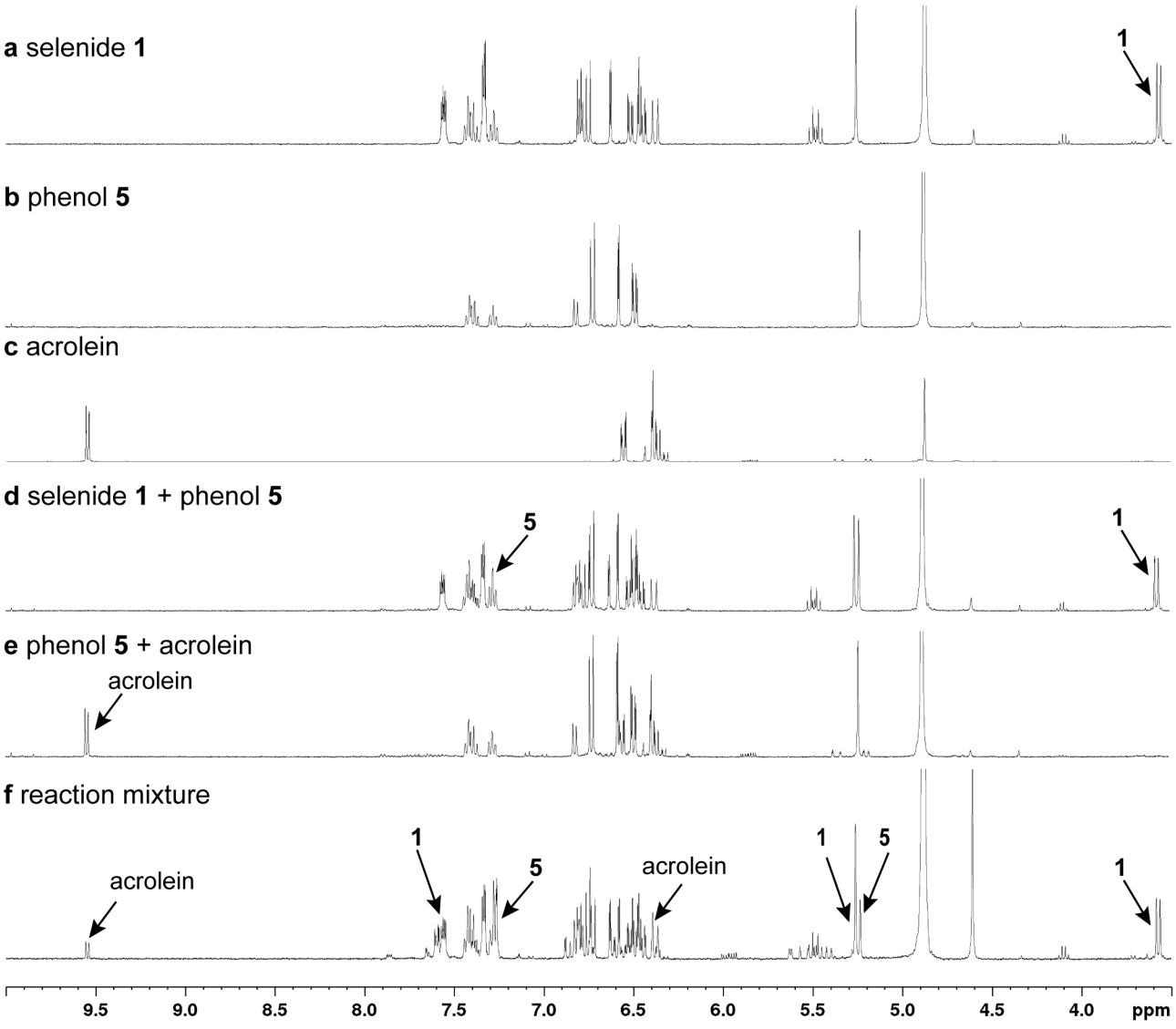

Figure 3. Mechanistic studies ^{1}H NMR (400 MHz, CD_3OD) spectra of (a) selenide 1, (b) phenol **5**, (c), acrolein, (d) selenide **1** and phenol **5** (1:1), (e) acrolein and phenol **5** (1:1), (f) reaction mixture of selenide **1** and H_2O_2.

To investigate the mechanism of the reaction between selenide **1** and H_2O_2 as depicted in Figure 2A, we monitored the reaction in situ by ^{1}H NMR spectroscopy. Figure 3a-e show selenide **1**, phenol **5**, acrolein, a 1:1 mixture of **1** and **5**, and a 1:1 mixture of **5** and acrolein in CD_3OD, respectively, Upon treatment of selenide **1** with substoichiometric amounts of H_2O_2, both phenol **5** and acrolein were formed (Figure 3f), supporting our proposed design for the H_2O_2 detection strategy. The HPLC chromatograms (Figure S1, Supporting Information) revealed that the reaction of selenide **1** with H_2O_2 produced phenol **5**, but did not produce $PhSeO_2H$. Therefore, pathway 1 (Figure 2A) is operative under these conditions leading to the formation of the putative intermediate PhSeOH as a side product.

Since organic selenides are prone to oxidation in air,[12] we investigated the stability of **1** under ambient conditions. The ^{1}H NMR analysis of **1** in DMSO-d_6 showed that **1** underwent cis-trans isomerization of the enol ether with a half-life of 60 days (Figures S2 and S3, Supporting Information). Even so, the compound was quite resistant to oxidative decomposition up to 60 days as manifested by the presence of only less than 10% acrolein.

As evident from Figure S4 and Table S1 (Supporting Information), the difference in fluorescence intensity of probe **1** and phenol **5**, is 27-fold. Generally, *O*-alkylation of Pittsburgh Green suppresses the fluorescence by 200–400 fold.[13] The somewhat modest fluorescence increase in the current system is attributed to the trace contamination of the fluorescent compound **5** during the purification of the non-fluorescent probe **1**. From the standard calibration curve (Figure S4), the estimated amount of **5** in **1** as an impurity was calculated to be 2.5%, leading to a 5–10 times higher background signal. Thus, if trace phenol **5** can be removed from selenide **1** (HPLC did not improve the purity of **1**), the signal increase in the conversion of **5** to **1** should be 125–250 fold. Nevertheless, the trace amount of **5** in **1** does not affect the calculation of rate constant shown below (Figure 4).

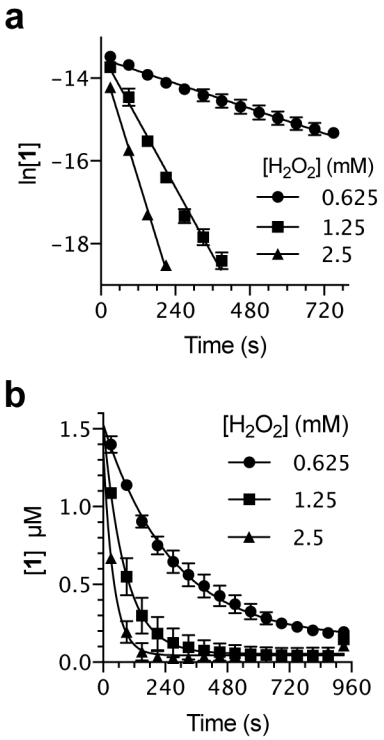

Figure 4. (a) plot of ln[**1**] vs t to obtain slope (k') and (b) plot of [**1**] vs time. For (a), Y = -0.002514X – 13.52 (R^2 = 0.8939) for 0.625 mM H_2O_2, Y = -0.01359X – 13.38 (R^2 = 0.9792) for 1.25 mM H_2O_2, and Y = -0.02432X – 13.51 (R^2 = 0.9978) for 2.5 mM H_2O_2.

With the fluorometrically measured concentrations of selenide **1** shown in Table S3 (Supporting Information), ln[**1**] versus time (s) was plotted to obtain observed rate constants k' as the slope of the linear plot (Figure 4a). To determine the second-order rate constant of the reaction of **1** with H_2O_2, a solution of **1** in 5%

MeCN in a pH 7.5 HEPES buffer was treated with H_2O_2 in a 96-well plate, and the progressive increase in fluorescence was recorded measured every minute until the reaction was completed. The fluorescence readout was converted to the amount of phenol **5** formed using Figure S5. Based on the pseudo first-order kinetic studies (Figure 4b), the second-order rate constant *k* of the reaction was calculated (details in Supporting Information, Figure S6 and Table S3) to be 9.82 ± 1.11 $M^{-1}s^{-1}$.

To verify that **1** could quantitatively measure H_2O_2 concentrations, we incubated **1** with increasing concentrations of H_2O_2. Fluorescence increased linearly with H_2O_2 concentration (Figure 5a), indicating that the probe could be used to quantify H_2O_2.

Following the concentration dependence studies, the selectivity of **1** was assessed against $O_2^{\bullet-}$, $^1O_2$, •OH, ClO^-, $ONOO^-$, ^{t}BuOOH, NO_3^-, NO_2^-, and NO•. Relative to H_2O_2, little reaction was observed with other ROS and RNS (Figure 5b). The production of some of these ROS required H_2O_2 as a reagent or generated H_2O_2 as a product, for which we carefully performed control experiments (Supporting Information for details). For example, to determine whether the probe reacts with $O_2^{\bullet-}$, KO_2 was added to a solution of **1** buffered at pH 7 for 15 min and compared to the reaction with H_2O_2. Since $O_2^{\bullet-}$ is known to spontaneously dismutate to form H_2O_2, increasing amounts of catalase were added to the samples containing KO_2 to ensure that **1** did not react with any of the in-situ-generated H_2O_2. Selenide **1** reacted readily with H_2O_2, while the observed fluorescence from the samples containing KO_2 decreased with increasing catalase concentrations (Figure S7), indicating that **1** did not react with $O_2^{\bullet-}$. Therefore, **1** is selective for H_2O_2 over $O_2^{\bullet-}$.

$^1O_2$ was formed by the reaction of Na_2MoO_4 with H_2O_2.[14] A large fluorescence increase was observed only in the samples containing 100 μM of both Na_2MoO_4 and H_2O_2 (Figure S8). Fluorescence did not increase in samples containing only Na_2MoO_4, indicating that the probe was not reacting with the Na_2MoO_4. Together, these results suggested that the probe may have reacted with $^1O_2$. However, the addition of NaN_3, a known $^1O_2$ scavenger,[15] did not decrease the fluorescence. Thus, we concluded that the fluorescence increase was caused by the H_2O_2 required to produce $^1O_2$ and not by $^1O_2$ itself . 10^4 U/mL catalase was added to the solutions to verify that **1** indeed responded to excess H_2O_2 that had not reacted with the Na_2MoO_4. The addition of catalase abolished the fluorescence signal observed in the presence of high concentrations of H_2O_2 (Figure S8).

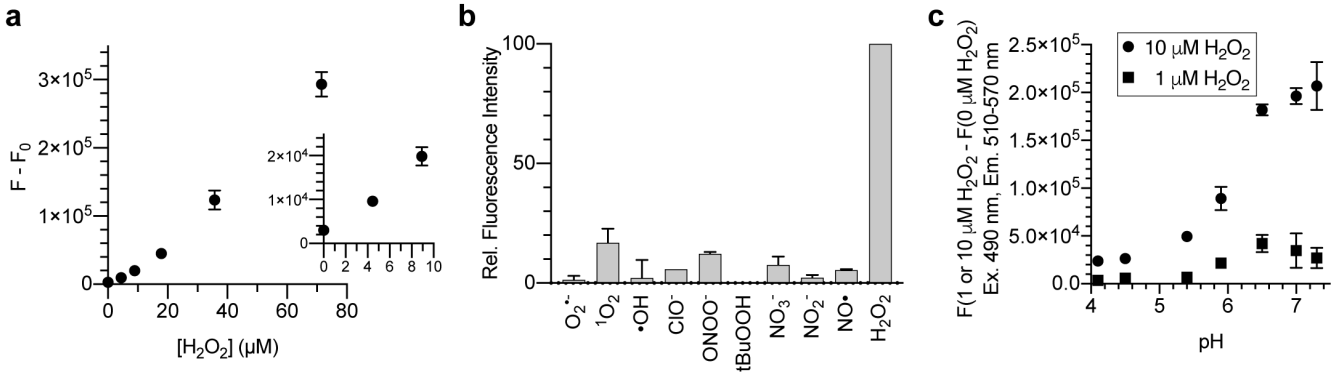

Figure 5. The fluorescence response of **1** (1 μM) at pH 7 (a) with increasing concentrations of H_2O_2 or (b) various ROS. (a) 10 μM **1**, 0–71.5 μM H_2O_2, 14.5:85.5 MeCN/50 mM phosphate pH 7, (b) Data were normalized so that the reaction of **1** and H_2O_2 was set to 100. Excess ROS and RNS compared to **1** was used. (c) The fluorescence response of **1** (10 μM) with H_2O_2 (0, 1, or 10 μM) at various pHs. 10 μM **1**, 1:9 MeOH/25 mM phosphate in water, 20 min. The y-axis shows (fluorescence intensity with 1 or 10 μM H_2O_2) - (fluorescence intensity with no H_2O_2).

The reactivity of **1** with •OH was also investigated. •OH was generated from the reaction of Fe^{2+} with H_2O_2.[16] A solution of **1** was titrated with $FeSO_4$ and H_2O_2. Fluorescence did not increase as the concentration of $FeSO_4$ increased (Figure S9), indicating that neither $FeSO_4$ nor the •OH reacted with the probe. Addition of catalase to the solution reduced fluorescence intensity, indicating that the enhanced signals were caused by the reaction of the probe with the H_2O_2 required to produce •OH.

Next, we tested whether OCl^-, $ONOO^-$ (peroxynitrite), and ^{t}BuOOH would react with **1**. No statistically significant increase in fluorescence intensity was observed with increasing concentrations of OCl^-. A slight increase in fluorescence intensity was observed with increasing $ONOO^-$ concentration (Figure S10). This may be attributed to trace amounts of H_2O_2 in the $ONOO^-$ solution.[17] Furthermore, $ONOO^-$ may be too unstable to last and react with **1** under aqueous conditions because, once protonated, has only a half-life of 1.9 s at pH 7.4.[18] ^{t}BuOOH did not produce fluorescence even at 10 μM (Figure S11). The minute or negligible fluorescence signals observed in these studies led us to conclude that the tested ROS do not interfere with the **1**-based fluorometric method for H_2O_2.

We then sought to determine whether RNS would react with **1** to produce fluorescence. The probe was exposed to either NO_2^-, NO_3^- (nitrate), or NO• at various concentrations. The fluorescence change over the first 15 min was reported for NO_2^- and NO_3^- in Figure S12 and S13, respectively. No concentration dependence was observed with either NO_2^- or NO_3^- indicating that **1** did not react with these RNS. Similar results were obtained for NO• (Figure S14). These data suggest that **1** did not react with NO_2^-, NO_3^-, nor NO•. Altogether, the fluorometric method is selective for H_2O_2.

We studied the probe's response to H_2O_2 in the pH 4–7.3 range to determine whether this technology would work in acidic and neutral intracellular environments, such as lysosomes (pH 5),[19] Golgi apparatus (pH 6.4–6.8),[20] mitochondria (pH 6.9–8.0),[20] and cytoplasm (pH 7.1–7.6).[20] The probe should ideally also work

under oxidative stress conditions, wherein pH decreases to 6.9–7.0.[21] We found that the fluorescence signals were higher when the pH was above 5.4 (Figure 5c). The lower signals under acidic conditions match the pH-fluorescence profile of phenol **5** (Figure S15) and are not related to efficiency of the conversion from **1** to **5**. Therefore, the fluorescence method is effective in most of the biologically relevant pH range.

We then attempted to image H_2O_2 within cells. HeLa cells were incubated with 0.5 μM **1** for 15 min prior to imaging. After washing with HBSS and replacing the media, H_2O_2 was added. Within 30 s, a significant increase in fluorescence was observed in HeLa cells (Figure 6a). Punctate fluorescence in cytoplasm suggested that **1** might localize within mitochondria.

After detecting exogenously added H_2O_2 in cells, we focused our studies on more biologically relevant, endogenous H_2O_2. We attempted to monitor endogenous H_2O_2 production upon stimulation with ionomycin in RAW cells.[22] When ionomycin was added in the presence of the most widely used fluorescent probe for ROS, dihydrodichlorofluorescein acetate, fluorescence increase could hardly be observed (Figure S16). In contrast, with probe **1**, a significant response was observed within 30 s of addition of ionomycin relative to the baseline fluorescence (Figure 6b and Figure 6c) and peaked at 48 s. Therefore, not only did this experiment show the superiority with probe **1**, the kinetics of pharmacological H_2O_2 production was found to be much faster than previously thought.[23]

To study the localization of **1**, endothelial cells were simultaneously treated with **1** and MitoTracker Red for 20 min (Figure 6d). The first image taken 8 s after the addition of ionomycin already showed increased fluorescence, and time-lapse imaging showed that fluorescence continued to increase over time. The overlap of the green and red fluorescence indicated that the probe might be localizing to mitochondria. However, the Pearson correlation coefficient was 0.114 ± 0.034, suggesting that although some overlap with mitochondria was observed, the bulk of the green fluorescence was observed outside of mitochondria. Furthermore, the diffusion of both the green and red fluorescence indicated that stimulation with ionomycin likely induced changes in mitochondrial membrane potential or permeability causing the contents to leak out.

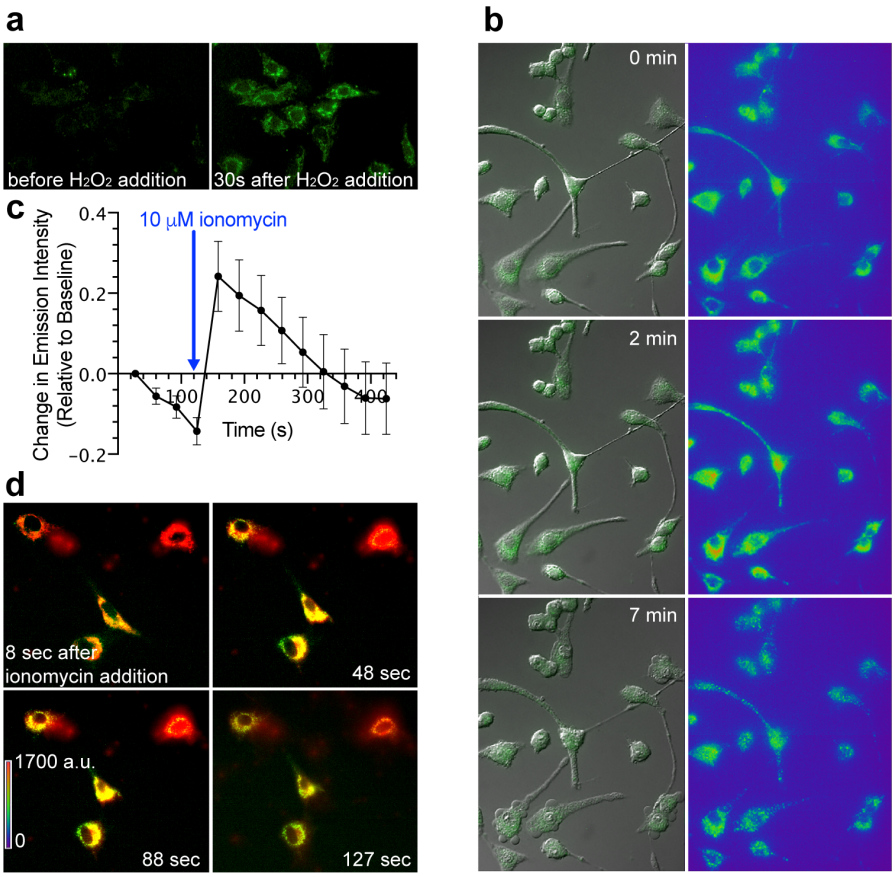

Figure 6. Cellular images using **1**. (a) HeLa cells treated with **1** showed a significant fluorescence increase after the addition of H_2O_2. Cells were loaded with **1** for 15 min and washed prior to imaging. H_2O_2 was added while imaging. (b) RAW macrophages loaded with 0.5 μM **1** showed (c) a significant response within 30 s of addition of ionomycin (final concentration: 10 μM). Fluorescence channel (green) and pseudo-color shown. (d) Endothelial cells loaded with **1** and MitoTracker Red were stimulated with ionomycin (final concentration: 10 μM). Colocalization studies revealed mildly increased green fluorescence intensity in mitochondria.

H_2O_2 has been recognized as a critical signaling molecule for the recruitment of immune cells for wound regeneration.[4] To date, only genetically encoded protein-based fluorescent probes have been able to illuminate the spatiotemporal dynamics of H_2O_2 for wound healing models in zebrafish.[4a] We hypothesized that our method might be rapid enough to match the protein-based imaging *in vivo*. As a platform to test this hypothesis, we applied **1** to image a zebrafish tail wound-healing model. Fish were loaded with probe **1** for 2 h before anesthetizing and mounting them in agarose. The tail fin was subsequently snipped, and the images were taken every 60 s. We observed an increase in fluorescence intensity, with the fluorescence at a maximum approximately 10–20 min after tail snipping. As shown in Figure 7 and the movie in the Supporting Information, the probe was capable of providing the spatiotemporal information that matches the previous report.[4a]

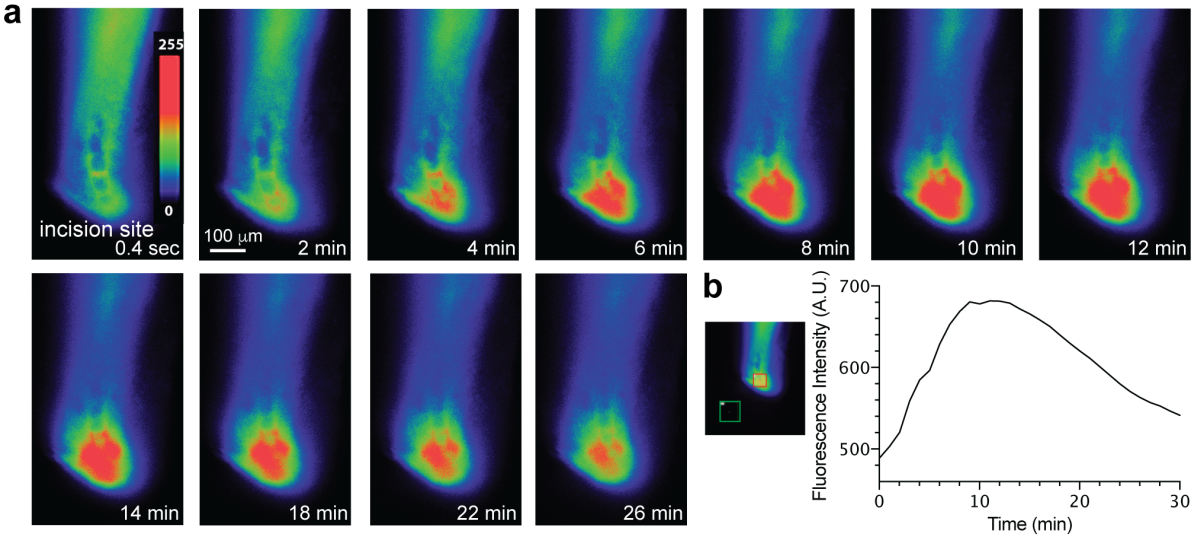

Figure 7. Imaging of H_2O_2 in zebrafish wound-healing model. (a) Snap shots of the fluorescence imaging of wound-induced H_2O_2. Zebrafish were loaded with **1**, then had the tails snipped. H_2O_2 was produced at the incision site over the course of 30 min. The original movies are available in the Supporting Information. (b) The fluorescence intensity over time. The Y-axis = fluorescence intensity in the red square – fluorescence intensity in the green square.

In conclusion, the reaction of the nonfluorescent selenide **1** with H_2O_2 forms the fluorescent phenol **5** via the oxidation/[2,3]-sigmatropic rearrangement/hydrolysis sequence. Selenide **1** reacts with H_2O_2 seven times faster than boronate-based probes. The second-order rate constant for the reaction of **1** with H_2O_2 was of the same order of magnitude as the reaction of thiols with H_2O_2, indicating that the detection of intracellular H_2O_2 is not severely hampered by endogenous thiols. This is consistent with the notion that the oxidation of selenium is faster than that of sulfur compounds.[24] Our careful control experiments ensured that we were monitoring the intended ROS. Selenide **1** was found to be selective for H_2O_2.

Selenide **1** instantaneously responded to both exogenously applied and endogenously produced H_2O_2, indicating its applicability in gaining spatiotemporal insights into cellular pathways involving H_2O_2. Ionomycin is a widely used reagent to intracellularly induce H_2O_2 in approximately 2 min.[23] We discovered that H_2O_2 was produced earlier (8–48 s) with ionomycin. Generally, chemical probes for H_2O_2 detect endogenously produced H_2O_2 later times (ca. 30 min). [7c, 7d, 7g, 8e] In the zebrafish tail wounding model, we observed the rapid generation of H_2O_2 near the wound site in real time using selenide **1**, recapitulating the results using a protein-based probe.[4a]

We acknowledge that two challenges exist with **1**. First, the fluorophore **5** diffuses throughout the cell, complicating studies that require extended time periods. Second, the pK_a of **5** is ~7 and thus the fluorescence signals are weakened under acidic conditions. Nonetheless, the use of seleno Mislow-Evans rearrangement may provide a new platform for fluorometric detection of intracellular H_2O_2.

Acknowledgements

This work was funded by US National Science Foundation Grants CHE-0911092 and CHE-1506942. We thank Dr. Steve Geib (University of Pittsburgh) for the X-ray analysis of **1** and Mr. Jevin M. Jupena (University of Pittsburgh) for the re-synthesis of probe **1**.

[1] (a) C. C. Winterbourn, *Nat. Chem. Biol.* **2008**, *4*, 278–286; (b) H. Sies, D. P. Jones, *Nat. Rev. Mol. Cell Biol.* **2020**, *10.1038/s41580-020-0230-3*.

[2] J. R. Stone, S. Yang, *Antioxid. Redox Signaling* **2006**, *8*, 243–270.

[3] (a) J. B. Bliska, D. S. Black, *Infect. Immun.* **1995**, *63*, 681–685; (b) K. M. Holmström, T. Finkel, *Nat. Rev. Mol. Cell Biol.* **2014**, *15*, 411–421; (c) F. Antunes, P. M. Brito, *Redox Biol.* **2017**, *13*, 1–7; (d) É. Dóka, T. Ida, M. Dagnell, Y. Abiko, N. C. Luong, N. Balog, T. Takata, B. Espinosa, A. Nishimura, Q. Cheng, Y. Funato, H. Miki, J. M. Fukuto, J. R. Prigge, E. E. Schmidt, E. S. J. Arnér, Y. Kumagai, T. Akaike, P. Nagy, *Sci. Adv.* **2020**, *6*, eaax8358; (e) S. F. Erttmann, N. O. Gekara, *Nat. Commun.* **2019**, *10*, 3493; (f) J.-F. Pei, X.-K. Li, W.-Q. Li, Q. Gao, Y. Zhang, X.-M. Wang, J.-Q. Fu, S.-S. Cui, J.-H. Qu, X. Zhao, D.-L. Hao, D. Ju, N. Liu, K. S. Carroll, J. Yang, E. E. Zhang, J.-M. Cao, H.-Z. Chen, D.-P. Liu, *Nat. Cell Biol.* **2019**, *21*, 1553–1564; (g) W. Qian, N. Kumar, V. Roginskaya, E. Fouquerel, P. L. Opresko, S. Shiva, S. C. Watkins, D. Kolodieznyi, M. P. Bruchez, B. Van Houten, *Proc. Natl. Acad. Sci. U. S. A.* **2019**, *116*, 18435–18444.

[4] (a) P. Niethammer, C. Grabher, A. T. Look, T. J. Mitchison, *Nature* **2009**, *459*, 996–999; (b) J. Pillay, V. M. Kamp, E. van Hoffen, T. Visser, T. Tak, J. W. Lammers, L. H. Ulfman, L. P. Leenen, P. Pickkers, L. Koenderman, *J. Clin. Invest.* **2012**, *122*, 327–336; (c) B. Enyedi, P. Niethammer, *Methods Enzymol.* **2013**, *528*, 237–255; (d) P. Martin, R. Nunan, *Brit. J. Dermatol.* **2015**, *173*, 370–378; (e) C. Dunnill, T. Patton, J. Brennan, J. Barrett, M. Dryden, J. Cooke, D. Leaper, N. T. Georgopoulos, *Int. Wound J.* **2017**, *14*, 89–96; (f) M. Jelcic, B. Enyedi, J. B. Xavier, P. Niethammer, *Biophys. J.* **2017**, *112*, 2011–2018; (g) B. Kunkemoeller, T. R. Kyriakides, *Antioxid. Redox Signaling* **2017**, *27*, 823–838; (h) A. Hervera, F. De Virgiliis, I. Palmisano, L. Zhou, E. Tantardini, G. Kong, T. Hutson, M. C. Danzi, R. B.-T. Perry, C. X. C. Santos, A. N. Kapustin, R. A. Fleck, J. A. Del Río, T. Carroll, V. Lemmon, J. L. Bixby, A. M. Shah, M. Fainzilber, S. Di Giovanni, *Nat. Cell Biol.* **2018**, *20*, 307–319; (i) P. Niethammer, *Semin. Cell Dev. Biol.* **2018**, *80*, 13–16; (j) M. M. G. Romero, G. McCathie, P. Jankun, H. H. Roehl, *Nat. Commun.* **2018**, *9*, 4010; (k) J. Chen, T. Yu, X. He, Y. Fu, L. Dai, B. Wang, Y. Wu, J. He, Y. Li, F. Zhang, J. Zhao, C. Liu, *Biochem. Biophys. Res. Commun.* **2019**, *516*, 680–685.

[5] (a) O. Myhre, J. M. Andersen, H. Aarnes, F. Fonnum, *Biochem. Pharmacol.* **2003**, *65*, 1575–1582; (b) M. M. Tarpey, I. Fridovich, *Circ. Res.* **2001**, *89*, 224–236; (c) A. Levine, R. Tenhaken, R. Dixon, C. Lamb, *Cell* **1994**, *79*, 583–593.

[6] K. N. Markvicheva, D. S. Bilan, N. M. Mishina, A. Y. Gorokhovatsky, L. M. Vinokurov, S. Lukyanov, V. V. Belousov, *Bioorg. Med. Chem.* **2011**, *19*, 1079–1084.

[7] (a) M. C. Y. Chang, A. Pralle, E. Y. Isacoff, C. J. Chang, *J. Am. Chem. Soc.* **2004**, *126*, 15392–15393; (b) B. C. Dickinson, Y. Tang, Z. Y. Chang, C. J. Chang, *Chem. Biol.* **2011**, *18*, 943–948; (c) U. Rodella, M. Scorzeto, E. Duregotti, S. Negro, B. C. Dickinson, C. J. Chang, N. Yuki, M. Rigoni, C. Montecucco, *Neurobiol. Dis.* **2016**, *96*, 95–104; (d) Y. Lu, X. Shi, W. Fan, C. A. Black, Z. Lu, C. Fan, *Spectrochim. Acta, Part A* **2018**, *190*, 353–359; (e) H. Wang, Z. X. He, Y. Y. Yang, J. Zhang, W. Zhang, W. Zhang, P. Li, B. Tang, *Chem. Sci.* **2019**, *10*, 10876-10880; (f) J. Pallu, C. Rabin, G. Creste, M. Branca, F. Mavre, B. Limoges, *Chem.-Eur. J.* **2019**, *25*, 7534–7546; (g) P. Hou, S. Chen, G. Liang, H. Li, H. Zhang, *Spectrochim. Acta, Part A* **2020**, *236*, 118338.

[8] (a) M. Abo, Y. Urano, K. Hanaoka, T. Terai, T. Komatsu, T. Nagano, *J. Am. Chem. Soc.* **2011**, *133*, 10629–10637; (b) A. P. Singh, K. M. Lee, D. P. Murale, T. Jun, H. Liew, Y. H. Suh, D. G. Churchill, *Chem. Commun.* **2012**, *48*, 7298–7300; (c) S. T. Manjare, Y. Kim, D. G. Churchill, *Acc. Chem. Res.* **2014**, *47*, 2985–2998; (d) Z. Lou, P. Li, K. Han, *Acc. Chem. Res.* **2015**, *48*, 1358–1368; (e) S. Ye, J. J. Hu, D. Yang, *Angew. Chem., Int. Ed.* **2018**, *57*, 10173–10177; (f) B. Li, J.-B. Chen, Y. Xiong, X. Yang, C. Zhao, J. Sun, *Sens. Actuators, B* **2018**, *268*, 475–484; (g) D.-J. Zheng, Y.-S. Yang, H.-L. Zhu, *Trends Anal. Chem.* **2019**, *118*, 625–651.

[9] (a) P. Bickart, F. W. Carson, J. Jacobus, E. G. Miller, K. Mislow, *J. Am. Chem. Soc.* **1968**, *90*, 4869–4876; (b) D. A. Evans, G. C. Andrews, *Acc. Chem. Res.* **1974**, *7*, 147–155; (c) H. J. Reich, *J. Org. Chem.* **1975**, *40*, 2570–2572.

[10] B. J. Albert, A. Sivaramakrishnan, T. Naka, N. L. Czaicki, K. Koide, *J. Am. Chem. Soc.* **2007**, *129*, 2648–2659.

[11] P. A. Grieco, S. Gilman, M. Nishizawa, *J. Org. Chem.* **1976**, *41*, 1485–1486.

[12] A. Krief, F. Lonez, *Tetrahedron Lett.* **2002**, *43*, 6255–6257.

[13] S. Ando, K. Koide, *J. Am. Chem. Soc.* **2011**, *133*, 2556–2566.

[14] G. Chen, F. Song, J. Wang, Z. Yang, S. Sun, J. Fan, X. Qiang, X. Wang, B. Dou, X. Peng, *Chem. Commun.* **2012**, *48*, 2949–2951.

[15] (a) K. Yamada, T. Ono, H. Nishioka, *J. Radiat. Res.* **1996**, *37*, 29–37; (b) M. Osada, Y. Ogura, H. Yasui, H. Sakurai, *Biochem. Biophys. Res. Commun.* **1999**, *263*, 392–397.

[16] E. W. Miller, A. E. Albers, A. Pralle, E. Y. Isacoff, C. J. Chang, *J. Am. Chem. Soc.* **2005**, *127*, 16652–16659.

[17] G. Merényi, J. Lind, G. Czapski, S. Goldstein, *Proc. Natl. Acad. Sci. U. S. A.* **2000**, *97*, 8216–8218.

[18] J. S. Beckman, T. W. Beckman, J. Chen, P. A. Marshall, B. A. Freeman, *Proc. Natl. Acad. Sci. U. S. A.* **1990**, *87*, 1620–1624.

[19] S.-S. Li, M. Zhang, J.-H. Wang, F. Yang, B. Kang, J.-J. Xu, H.-Y. Chen, *Anal. Chem.* **2019**, *91*, 8398–8405.

[20] J. Llopis, J. M. McCaffery, A. Miyawaki, M. G. Farquhar, R. Y. Tsien, *Proc. Natl. Acad. Sci. U. S. A.* **1998**, *95*, 6803–6808.

[21] W. Shi, X. Li, H. Ma, *Angew. Chem., Int. Ed.* **2012**, *51*, 6432–6435.

[22] E. J. Swindle, J. A. Hunt, J. W. Coleman, *J. Immunol.* **2002**, *169*, 5866–5873.

[23] C. Dahlgren, A. Johansson, K. Orselius, *Biochimica et Biophysica Acta* **1989**, *1010*, 41–48.

[24] Advanced Organic Chemistry: Reaction Mechanisms By Reinhard Bruckner, 1st edition, Page 573 Chapter 14

Table of Content figure

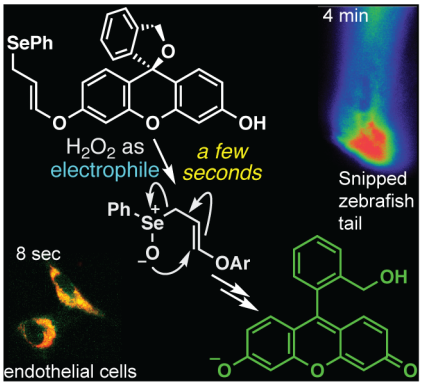

Table of Contents

General Techniques S2

Synthesis of **1** S2

Mechanistic studies S4

HPLC chromatogram of selenide **1** and phenol **5** S4

Stability studies S6

Determination of the difference in fluorescence intensity between selenide **1** and phenol **5** S7

Pseudo first order kinetics and evaluation of second order rate constant S8

Raw data for studying pseudo first order kinetics S9

Reaction of **1** with H_2O_2 ..... S10

Determining selectivity of **1**: Reaction with $O_2^{\bullet-}$ S10

Determining selectivity of **1**: Reaction with $^1O_2$ S11

Determining selectivity of **1**: Reaction with •OH S12

Determining selectivity of **1**: Reaction with ClO^- and $ONOO^-$ S13

Determining selectivity of **1**: Reaction with ^{t}BuOOH S13

Determining selectivity of **1**: Reaction with NO_2^- S14

Determining selectivity of **1**: Reaction with NO_3^- S14

Determining selectivity of **1**: Reaction with NO• S15

pH dependence of the reaction of **1** with H_2O_2 ..... S16

pH dependence of phenol **5** S16

Cellular Imaging S18

Zebrafish tail-wounding model S18

References S18

Author Contributions S18

Spectrum 1. ^{1}H NMR spectrum of **8** (300 MHz, $CDCl_3$, 293K). S19

Spectrum 2. ^{13}C NMR spectrum of **8** (100 MHz, $CDCl_3$, 293K). S20

Spectrum 3. ^{1}H NMR spectrum of **9** (300 MHz, $CDCl_3$, 293K). S21

Spectrum 4. ^{13}C NMR spectrum of **9** (100 MHz, $CDCl_3$, 293K). S22

Spectrum 5. ^{1}H NMR spectrum of **1** (300 MHz, $CDCl_3$, 293K). S23

Spectrum 6. ^{13}C NMR spectrum of **1** (100 MHz, $CDCl_3$, 293K). S24

General Techniques

All reactions were carried out with freshly distilled solvents under anhydrous conditions, unless otherwise noted. All of the flasks used for carrying out reactions were dried in an oven at 80 °C prior to use. Unless specifically stated, the temperature of a water bath during the evaporation of organic solvents using a rotary evaporator was about 35 ± 5 °C. All of the syringes in this study were dried in an oven at 80 °C and stored in a desiccator over Drierite®. Tetrahydrofuran (THF) was distilled over sodium metal and benzophenone. Methylene chloride (CH_2Cl_2) was distilled over calcium hydride. Acetonitrile was distilled from CaH_2 and stored over 3Å molecular sieves. Yields refer to chromatographically and spectroscopically (^{1}H NMR) homogenous materials, unless otherwise stated. All reactions were monitored by thin-layer chromatography (TLC) carried out on 0.25-mm Merck silica gel plates (60F-254) using UV light (254 nm) for visualization or a solution of anisaldehyde in ethanol or a solution of 2.4% phosphomolybdic acid, 1.4% phosphoric acid, and 5% sulfuric acid in water as a developing agents and heat for visualization. Silica gel (230–400 mesh) was used for flash column chromatography. A rotary evaporator was connected to a water aspirator that produced a vacuum pressure of approximately 60 mmHg when it was connected to the evaporator. NMR spectra were recorded on a Bruker Advance spectrometer at 300 MHz or 400 MHz. The chemical shifts are given in parts per million (ppm) on a delta (δ) scale. The solvent peak was used as a reference value: for ^{1}H NMR: $CHCl_3$ = 7.27 ppm, CH_3OH = 3.31 ppm, CH_3CN = 2.08 ppm; for ^{13}C NMR: $CDCl_3$ = 77.00 ppm, CD_3OD = 49.00 ppm, and CD_3CN = 1.79 ppm for CD_3 or 118.26 ppm for CN. The following abbreviations are used to indicate the multiplicities: s = singlet; d = doublet; t = triplet; q = quartet; m = multiplet; br = broad. High-resolution mass spectra (HRMS) were recorded on a VG 7070 spectrometer. Infrared (IR) spectra were collected on a Mattson Cygnus 100 spectrometer. Samples for acquiring IR spectra were prepared as a thin film on a NaCl plate by dissolving the compound in CH_2Cl_2 and then evaporating the CH_2Cl_2.

All fluorescence measurements (excitation 490 nm, emission 510–570 nm) were carried out using a Promega Biosystems Modulus II Microplate Reader or a HoribaMax Fluorometer unless otherwise stated. Data analysis was performed using GraphPad Prism 8.

Synthesis of 1

Methyl (*E*)-2-(6-((3-methoxy-3-oxoprop-1-en-1-yl)oxy)-3-oxo-3*H*-xanthen-9-yl)benzoate (8)

A suspension of **7**[1] (7.760 g, 22.52 mmol) in dry CH_2Cl_2 (390 mL) was treated with *N*-methylmorpholine (683 mg, 6.76 mmol) and methyl propiolate (9.467 mg, 112.6 mmol) under a nitrogen atmosphere at 23 °C. After stirring the reaction mixture for 24 h at the same temperature, silica gel (24 g) was added, and the mixture was concentrated *in vacuo*. The resulting crude residue was purified by flash column chromatography (10→90% EtOAc in hexanes) on silica gel (560 mL) to obtain vinyl ether **8** (7.65 g, 79%) as an orange solid. *Data for* **8**: m.p.: 192.0–193.0 °C; R_f: 0.25 (70% EtOAc in hexanes); IR (film): ν_{max} = 3060, 2923, 1722 (C=O), 1642 (C=O), 1639 (C=O), 1595, 1522, 1444, 1378, 1267, 1247, 1191, 1158, 1133, 1106, 1081, 854, 707 cm^{-1}; ^{1}H NMR (300 MHz, $CDCl_3$, 293 K): δ 8.25 (dd, *J* = 7.5, 1.5 Hz, 1H), 7.85 (d, *J* = 12.0 Hz, 1H), 7.79 (ddd, *J* = 7.5, 7.5, 1.2 Hz, 1H), 7.72 (ddd, *J* = 7.5, 7.5, 1.2 Hz, 1H), 7.33 (dd, *J* = 7.5, 1.2 Hz, 1H), 7.18 (d, *J* = 2.4 Hz, 1H), 6.98 (d, *J* = 9.0 Hz, 1H), 6.89 (dd, *J* = 9.6, 1.8 Hz, 1H), 6.87 (d, *J* = 9.6 Hz, 1H), 6.56 (dd, *J* = 9.6, 1.8 Hz, 1H), 6.46 (d, *J* = 1.8 Hz, 1H), 5.79 (d, *J* = 12.0 Hz, 1H), 3.76 (s, 3H), 3.66 (s, 3H); ^{13}C NMR (100 MHz, $CDCl_3$, 293 K): δ 185.9, 166.8, 165.5, 158.9, 158.5, 156.1, 153.4, 148.7, 134.3, 132.9, 131.3, 130.7, 130.6, 130.3, 130.2, 129.9, 129.3, 119.2, 118.0, 114.1, 106.3, 105.1, 104.7, 52.5, 51.6; HRMS (ESI-TOF) *m/z*: [M + H]+ calcd. for $C_{25}H_{19}O_7$ 431.1110, found 431.1125.

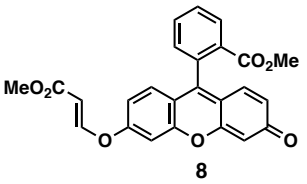

8

(*S,E*)-6'-((3-Hydroxyprop-1-en-1-yl)oxy)-3*H*-spiro[isobenzofuran-1,9'-xanthen]-3'-ol (9)

A 1 M solution of diisobutylaluminum hydride in hexanes (1.80 mL, 1.80 mmol) was added dropwise to a flask containing ester **8** (100 mg, 0.23 mmol) in dry CH_2Cl_2 (1.5 mL) under a nitrogen atmosphere at -78 °C. After stirring the reaction mixture for 15 min at the same temperature, the flask was warmed to 23 °C. The mixture was stirred at the same temperature for an additional 2 h, and then the reaction was quenched with 1 M aqueous sodium potassium tartrate (2 mL) at 0 °C. After stirring the mixture for 3 h at 23 °C, Et_2O (5 mL) and DDQ (57 mg, 0.25

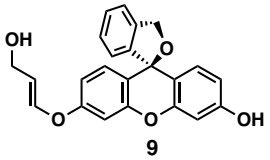

9

mmol) were added at 0 °C and the resulting mixture was stirred at the same temperature for 1 h. The combined organic and aqueous layers were filtered through a pad of Celite, and the pad was rinsed with EtOAc. The filtrate was dried under Na_2SO_4, filtered through a cotton plug, and concentrated *in vacuo*. The resulting crude residue was purified by flash column chromatography (10→60% EtOAc in hexanes) on silica gel (20 mL) to obtain alcohol **9** (57 mg, 66%) as a pale yellow solid and byproduct **5** (14 mg, 20%) as an orange solid. *Data for* **9***:* m.p.: 169.0–170.0 °C; R_f: 0.52 (70% EtOAc in hexanes); IR (film): ν_{max} = 3378 (O–H), 2923, 2853, 1673, 1601, 1480, 1434, 1409, 1266, 1173, 1114, 1004, 926, 854, 722 cm^{-1}; ^1H NMR (300 MHz, 1% CD_3OD in $CDCl_3$, 293 K): δ 7.36–7.37 (m, 2H), 7.23–7.28 (m, 1H), 6.91 (d, *J* = 2.4 Hz, 1H), 6.88 (br s, 1H), 6.84 (d, *J* = 2.4 Hz, 1H), 6.77 (d, *J* = 8.4 Hz, 1H), 6.68–6.70 (m, 1H), 6.70 (dt, *J* = 12.0, 1.8 Hz, 1H), 6.60 (d, *J* = 2.4 Hz, 1H), 6.52 (dd, *J* = 8.7, 2.4 Hz, 1H), 5.57 (dt, *J* = 12.0, 7.2 Hz, 1H), 5.29 (s, 2H), 4.15 (dd, *J* = 7.2, 1.8 Hz, 2H); ^{13}C NMR (100 MHz, $CDCl_3$, 293 K): δ 157.4, 157.1, 151.4, 151.3, 144.8, 144.3, 138.7, 130.1, 130.0, 128.5, 128.2, 123.9, 120.7, 119.0, 116.0, 112.9, 112.1, 111.6, 103.9, 102.7, 83.9, 71.8, 59.6; HRMS (ESI-TOF) *m/z*: [M + H]+ calcd. for $C_{23}H_{19}O_5$ 375.1227, found 375.1209.

(*S*,*E*)-6'-((3-(Phenylselanyl)prop-1-en-1-yl)oxy)-3*H*-spiro[isobenzofuran-1,9'-xanthen]-3'-ol (1)

A 10-mL round-bottomed flask equipped with a Teflon-coated magnetic stir bar containing **9** (85 mg, 0.23 mmol) was purged with argon. The flask was treated with THF (1.2 mL), $^nBu_3P$ (67 µL, 0.27 mmol), and PhSeCN (29 µL, 0.23 mmol) sequentially at 0 °C. The mixture was stirred at the same temperature for 30 min and was then quenched with sat. NH_4Cl. The quenched mixture was extracted with EtOAc (3 × 15 mL). The combined organic layers were dried over Na_2SO_4 and concentrated *in vacuo*. The resulting crude residue was purified by flash column chromatography (SiO_2, eluent: 5%→25% EtOAc in hexanes; 30 mL each) to obtain **1** (48 mg, 41%) as pale-yellow solid.

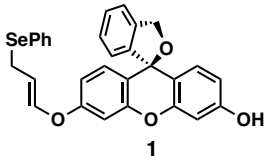

1

Data for **1**: m.p.: 125.5–126.5 °C; R_f: 0.56 (40% EtOAc in hexanes); IR (film): ν_{max} = 3286 (broad, O-H), 2923, 2853, 2360, 1664, 1609, 1496, 1458, 1427, 1331, 1266, 1247, 1210, 1177, 1111, 997, 928, 846, 804, 757, 737, 691 cm^{-1}; ^1H NMR (300 MHz, 1% CD_3OD in $CDCl_3$, 293 K): δ 7.56 (dd, *J* =6.0, 1.2 Hz, 2H), 7.36–7.34 (m, 2H), 7.32–7.31 (m, 3H), 7.27–7.26 (m, 1H), 6.88 (d, *J* = 7.5 Hz, 1H), 6.83 (dd, *J* = 8.1, 8.1 Hz, 2H), 6.66 (d, *J* = 2.4 Hz, 1H), 6.54 (m, 3H), 6.30 (d, *J* = 12.0 Hz, 1H), 5.57 (dt, *J* = 12.0, 8.4 Hz, 1H), 5.27 (s, 2H), 3.45 (dd, *J* = 8.1, 0.9 Hz, 2H); ^{13}C NMR (100 MHz, $CDCl_3$, 293 K): δ 157.5, 156.5, 151.4, 151.3, 144.6, 143.1, 139.0, 134.4, 133.2, 130.1, 130.0, 129.4, 129.2, 128.9, 128.5, 128.2, 127.7, 123.9, 120.7, 119.1, 117.0, 112.5, 111.9, 110.5, 103.6, 102.7, 83.6, 72.0, 25.6; HRMS (ESI-TOF) *m/z*: [M - H]+ calcd. for $C_{29}H_{21}O_4Se$ 513.0610, found 513.0610.

Mechanistic studies

Probe **1** (1.8 mg) in CD_3OD (0.75 mL) was treated with 943 mM H_2O_2 (1.9 µL). The crude reaction mixture was monitored in situ by ^1H NMR spectroscopy and analyzed against known standards (**5** and acrolein). Figure 3 shows that both **5** and acrolein were formed during the reaction.

HPLC chromatogram of selenide 1 and phenol 5

Column: Agilent 1200 system; Flow rate: 0.6 mL/min; Max. Pressure (bar): 600
Elution conditions: H_2O/MeCN 95:5 to 20:80, 0–15 min; 20:80 to 0:100, 15–20 min; 0:100, 20–25 min; 0:100 to 95:5, 25–30 min
Retention time for **1**: 20.1 min
Retention time for **5**: 27.6 min

(a)

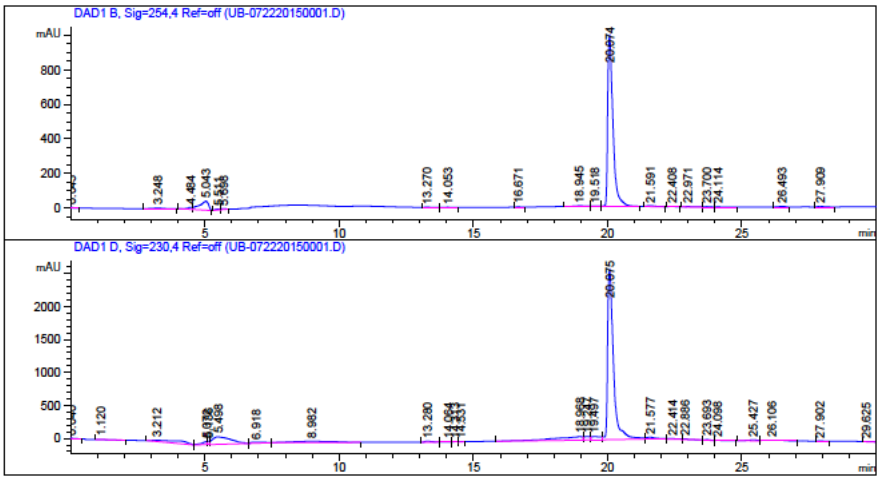

(b)

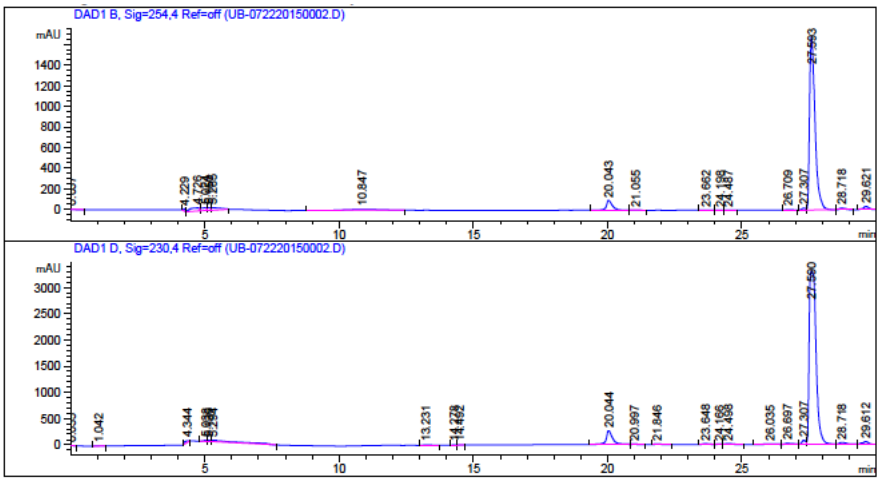

(c)

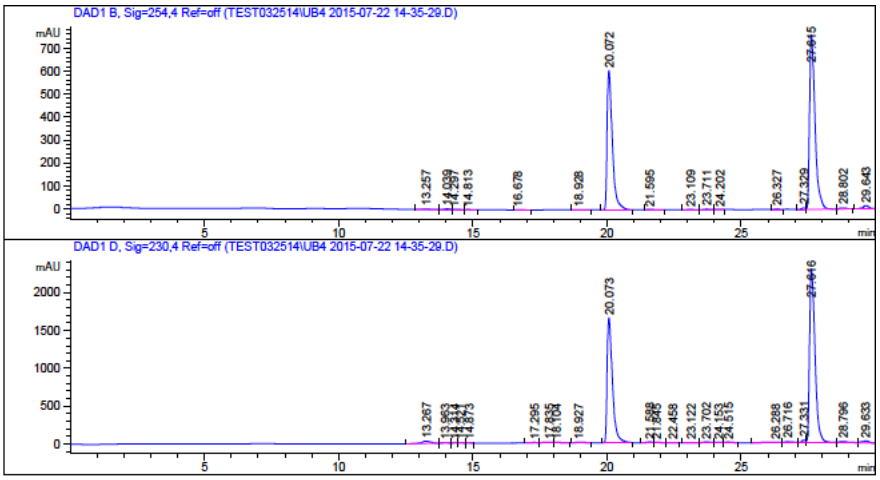

(d)

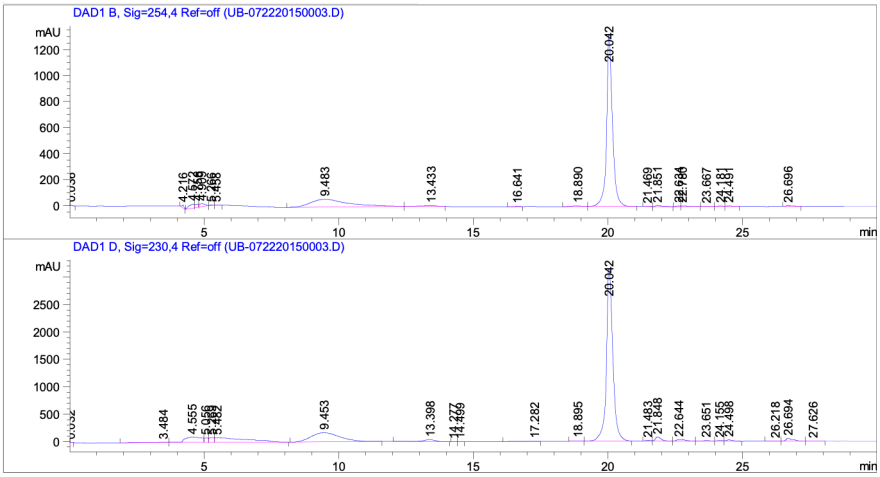

(e)

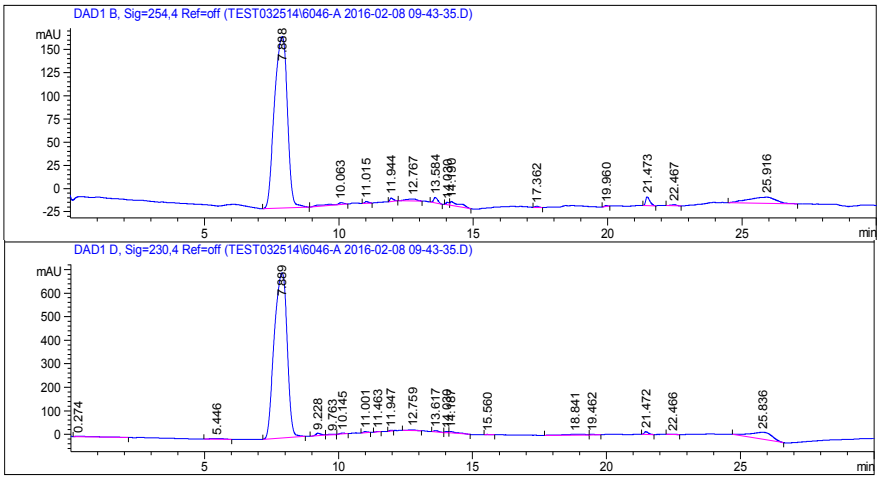

Figure S1. HPLC chromatograms of (a) authentic sample of selenide **1** (b) phenol **5** (c) selenide **1** + phenol **5** (d) crude reaction mixture of selenide **1** + 1 equiv H_2O_2, and (e) authentic sample of $PhSeO_2H$ acquired at λ = 254 nm and 230 nm, respectively.

Stability studies

To study the stability of **1**, the ^{1}H NMR spectra of **1** in DMSO-d_6 were obtained at specified intervals (days 1, 7, 14, 21, 30 and 60). The solution was left at room temperature and in air throughout the entire period.

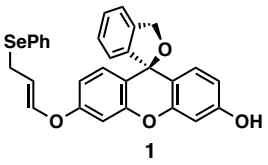

1

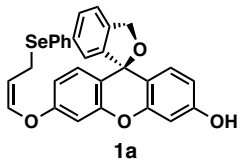

1a

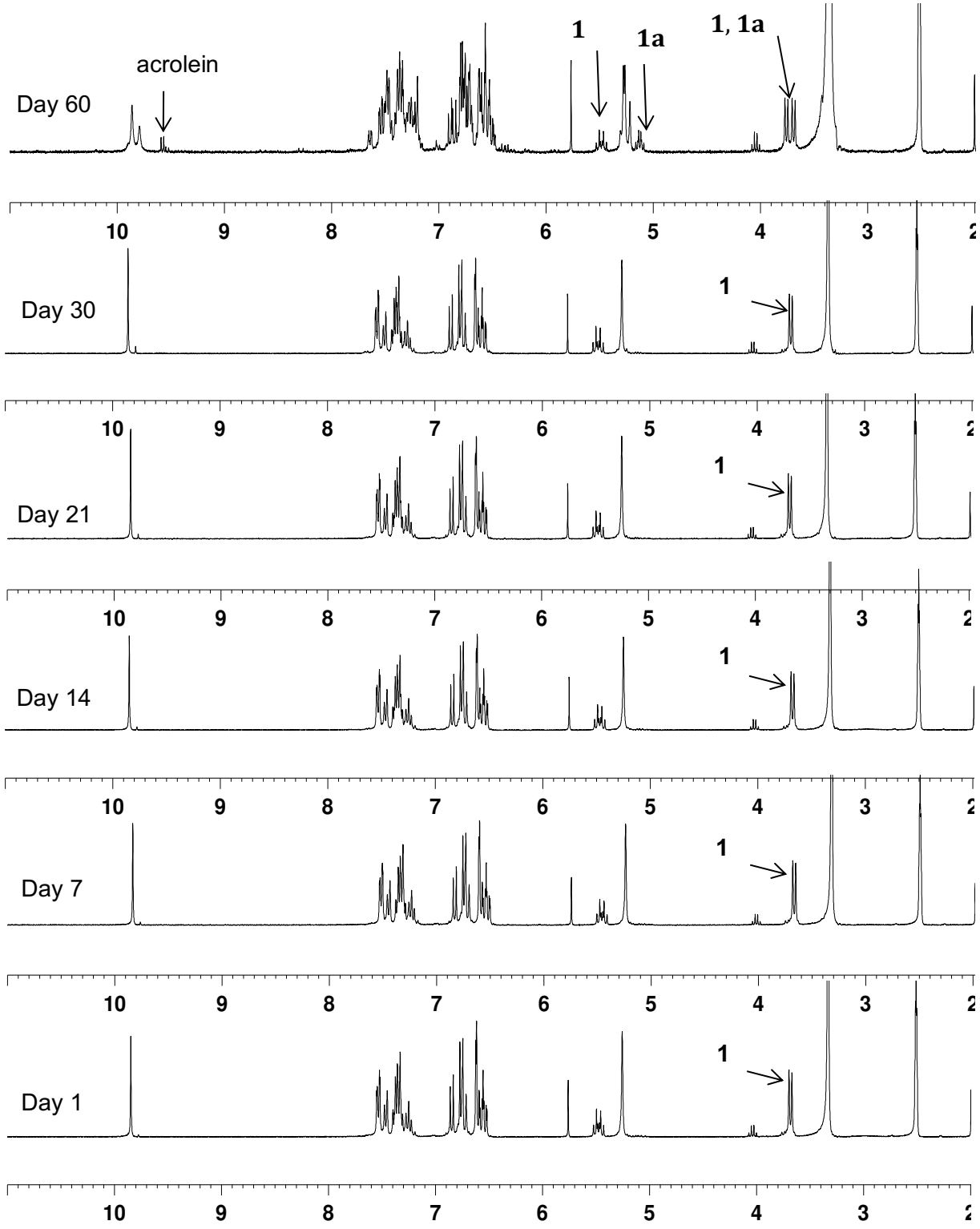

Figure S2. ^{1}H NMR spectra (300 MHz, DMSO-d_6) of **1** recorded on days 1, 7, 14, 21, 30 and 60.

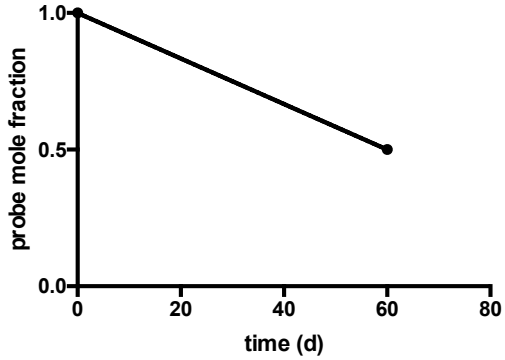

Figure S3. Half-life of probe **1**.

Determination of the difference in fluorescence intensity between selenide 1 and phenol 5

Solutions containing ultrapure water (681 µL), 1.2 M phosphate pH 7 buffer (31 µL), DMSO (28.1 µL), and 80 µM **1** or phenol **5** in DMSO (9.4 µL) were made. Aliquots of these solutions (200 µL) were transferred to the wells of a black 96-well plate and the fluorescence was measured.

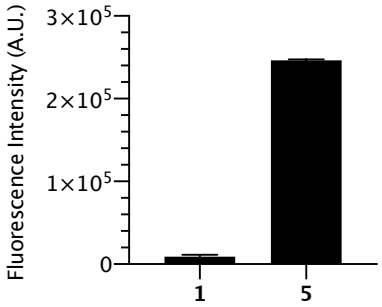

Figure S4. Difference in fluorescence intensity between selenide **1** and phenol **5**.

Compound	Fluorescence Intensity		
1	7,053	11,524	8,556
5	244,687	247,204	246,848

Table S1. Raw fluorescence values for Figure S4. *n* = 3.

Pseudo first order kinetics and evaluation of second order rate constant

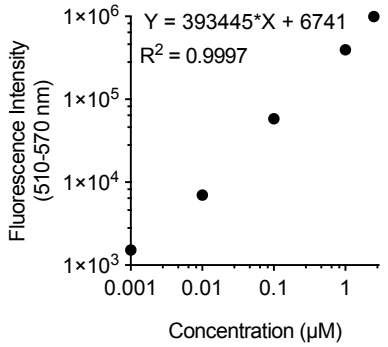

Figure S5. Calibration curve for phenol **5** shown on a log scale: 200 μL, 5% MeCN in 50 mM pH 7.5 HEPES buffer. *n* = 2. Error bars are invisible because they are smaller than the dots.

Best-fit values	
Slope	393445 ± 2396
Y-intercept when X=0.0	6741 ± 2887
X-intercept when Y=0.0	-0.01713
1/slope	2.54E-06
95% Confidence Intervals	
Slope	387921 to 398969
Y-intercept when X=0.0	84.06 to 13397
X-intercept when Y=0.0	-0.03434 to -0.0002119
Goodness of Fit	
R square	0.9997
Sy.x	7307
Is slope significantly non-zero?	
F	26975
DFn, DFd	1.000, 8.000
P value	< 0.0001
Deviation from zero?	Significant
Data	
Number of X values	5
Maximum number of Y replicates	2
Total number of values	10
Number of missing values	0
Equation	Y = 393445*X + 6741

F_0= 24616 units

	F-F_0 (515 nm); [H_2O_2] = 0.625 mM			F-F_0 (515 nm); [H_2O_2] = 1.25 mM			F-F_0 (515 nm); [H_2O_2] = 2.5 mM		
Time (s)	Expt. 1	Expt. 2	Expt. 3	Expt. 1	Expt. 2	Expt. 3	Expt.1	Expt. 2	Expt. 3
30	145,691	101,161	83,026	255,659	258,915	225,047	425,024	405,551	398,309
90	220,196	277,036	236,883	364,712	517,271	484,926	539,467	612,814	630,136
150	301,900	391,059	348,470	463,364	607,290	590,662	601,940	657,981	671,943
210	355,049	458,596	422,910	514,663	641,798	639,332	627,168	666,435	680,181
270	390,358	499,861	473,964	549,297	656,229	660,178	636,230	665,190	679,336
330	421,561	522,358	509,584	572,635	661,539	664,254	638,753	666,173	674,138
390	450,025	534,705	536,252	589,797	665,178	666,753	641,141	663,899	664,993
450	477,638	541,922	555,207	601,493	663,842	669,367	640,270	661,893	664,413
510	501,767	546,290	569,868	606,377	663,608	673,539	639,383	659,509	664,003
570	524,121	550,122	581,518	612,207	662,594	675,671	637,346	658,746	663,104
630	543,908	551,490	591,076	614,405	663,947	677,477	637,422	656,826	661,222
690	559,985	551,741	599,176	616,203	663,123	679,640	636,174	654,911	659,002
750	570,897	553,475	603,780	616,371	663,595	679,888	634,294	654,494	657,410
810	580,693	553,568	609,902	614,783	663,765	683,016	631,953	653,606	654,988
870	587,536	552,326	614,108	614,819	662,173	685,799	631,346	651,140	655,338

Table S2. Raw data for Figure 4a.

Raw data for studying pseudo first order kinetics

Rate= k'[**1**]; where k'= k[H_2O_2]

Final concentration: [H_2O_2] = 0.625 mM, 1.25 mM and 2.5 mM; [**1**] = 1.7 μM; 5% MeCN in pH 7.5 HEPES buffer 50 mM. All reactions were performed in triplicate in a 96-well plate.

Calculating [**1**] from the standard curve of **5**. Fluorescence Intensity = 393445•[**5**] + 6741; R^2 = 0.9997.

	[**1**] μM [H_2O_2] = 0.625 mM			[**1**] μM [H_2O_2] = 1.25 mM			[**1**] μM [H_2O_2] = 2.5 mM		
Time (s)	Exp. 1	Exp. 2	Exp. 3	Exp. 1	Exp. 2	Exp. 3	Exp. 1	Exp. 2	Exp. 3
30	1.3453	1.4596	1.5061	1.0631	1.0547	1.1417	0.6285	0.6785	0.6971
90	1.1541	1.0082	1.1113	0.7833	0.3918	0.4748	0.3348	0.1466	0.1022
150	0.9444	0.7157	0.8249	0.5301	0.1608	0.2035	0.1745	0.0307	-0.005
210	0.8081	0.5424	0.6339	0.3985	0.0722	0.0786	0.1098	0.0090	-0.026
270	0.7175	0.4365	0.5029	0.3096	0.0352	0.0251	0.0865	0.0122	-0.024
330	0.6374	0.3787	0.4115	0.2497	0.0216	0.0146	0.0801	0.0097	-0.010
390	0.5643	0.3470	0.3431	0.2057	0.0122	0.0082	0.0739	0.0155	0.0127
450	0.4935	0.3285	0.2944	0.1757	0.0157	0.0015	0.0762	0.0207	0.0142
510	0.4316	0.3173	0.2568	0.1631	0.0163	-0.009	0.0784	0.0268	0.0153
570	0.3742	0.3075	0.2269	0.1482	0.0189	-0.014	0.0837	0.0288	0.0176
630	0.3234	0.3040	0.2024	0.1425	0.0154	-0.019	0.0835	0.0337	0.0224
690	0.2822	0.3033	0.1816	0.1379	0.0175	-0.024	0.0867	0.0386	0.0281
750	0.2542	0.2989	0.1698	0.1375	0.0163	-0.025	0.0915	0.0397	0.0322
810	0.2290	0.2986	0.1541	0.1416	0.0159	-0.033	0.0975	0.0419	0.0384
870	0.2115	0.3018	0.1433	0.1415	0.0200	-0.040	0.0991	0.0483	0.0375

Table S3. Raw data for Figure 4b.

$[H_2O_2]$ (mM)	Slope k' (s^{-1})
2.5	0.02432
1.25	0.01359
0.625	0.00251

Table S4. Slope (k') obtained from the plot of ln [**1**] vs time.

From Figure 4b, three values of k' were obtained for three different concentrations of H_2O_2. Under pseudo first order conditions, k' = k$[H_2O_2]$. So, a plot of observed rate constant k' vs $[H_2O_2]$ yielded the second order rate constant k as the slope of the linear plot. After all calculations, it was found that second order rate constant k = 9.82 ± 1.11 $M^{-1}s^{-1}$.

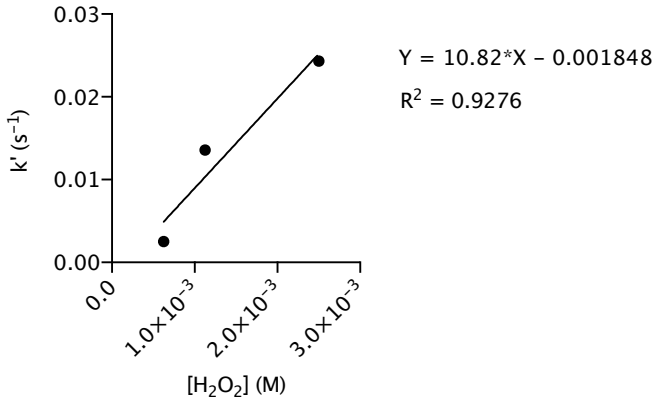

Figure S6. Plot of k' vs time to obtain second order rate constant k.

Reaction of 1 with H_2O_2

A solution of 0–159 µM H_2O_2 in 5:95 MeCN/50 mM phosphate pH 7 buffer (180 µL) was added to the wells of a black 96-well plate. A solution of 100 µM **1** in MeCN (20 µL) was then added to the wells. The solutions were allowed to incubate at 25 °C for 20 min before the fluorescence was measured.

Determining selectivity of 1: Reaction with $O_2^{\bullet-}$

A solution of 100 µM **1** in ethanol (20 µL) was added to 5:95 methanol/50 mM phosphate pH 7 buffer (140 µL). Then, either 0, 10, or 10^4 U/mL catalase (20 µL) was added to the mixtures. These solutions were transferred to centrifuge tubes containing solid potassium superoxide (~3 mg/sample). A control containing 100 µM **1** in ethanol (20 µL), 5:95 methanol/50 mM phosphate pH 7 buffer (160 µL), and 700 mM H_2O_2 (20 µL) was also generated. The solutions were allowed to incubate at 25 ˚C for 15 min prior to measuring fluorescence.

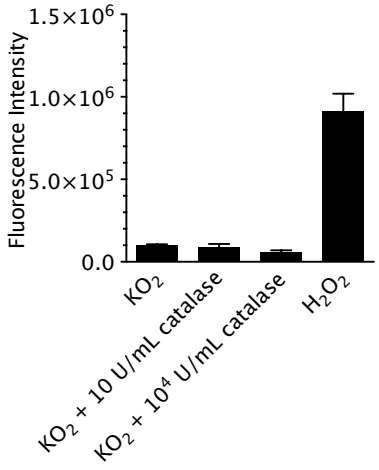

Figure S7. Determining selectivity of **1**: Reaction with $O_2^{\bullet-}$.

Sample	Fluorescence Intensity		
KO_2	106,099	92,938	99,300
KO_2 + 10 U/mL catalase	104,768	72,151	98,514
KO_2 + 10^4 U/mL catalase	63,553	41,950	67,009
H_2O_2	937,451	1,008,330	803,382

Table S5. Raw fluorescence values for determining selectivity of **1**: Reaction with $O_2^{\bullet-}$. *n* = 3.

Determining selectivity of 1: Reaction with $^1O_2$

Probe **1** was titrated with $NaMoO_4$ and H_2O_2 to determine whether $^1O_2$ reacted with the probe. A solution of 100 μM **1** in ethanol (20 μL) was added to 5:95 methanol/50 mM phosphate pH 7 buffer (140 μL). Water, 1 mM sodium azide, or 10^4 U/mL catalase (20 μL) was added to the mixture. $NaMoO_4$•$2H_2O$ (11.1 mg) was added to ultrapure water (2.00 mL). This solution was diluted to 20 μM, 200 μM, and 2.00 mM. H_2O_2 was diluted to 200 μM and 2.00 mM. Equal volumes of $NaMoO_4$ solution and H_2O_2 were added together, and an aliquot (20 μL) was immediately transferred to the solution containing **1**. The fluorescence intensity was measured immediately and again after incubation at 25 ˚C for 40 min.

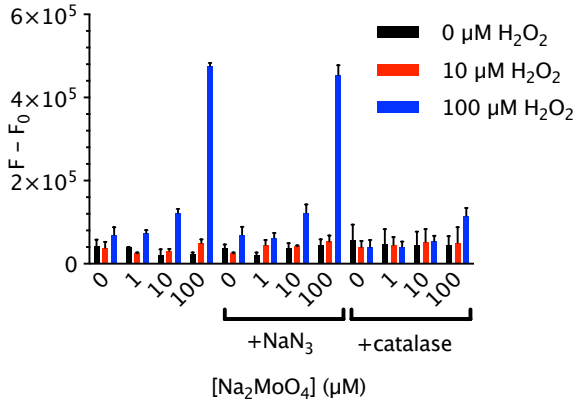

Figure S8. Determining selectivity of **1**: Reaction with $^1O_2$.

Additive	[$NaMoO_4$] (μM)	0 μM H_2O_2			10 μM H_2O_2			100 μM H_2O_2		
	0	59,711	30,413	38,407	34,413	26,177	54,164	86,970	68,803	48,948
	1	36,829	38,478	40,456	27,103	23,437	25,142	74,322	79,262	64,673
	10	1,067	29,637	27,490	33,243	34,233	26,543	132,450	119,014	113,217
	100	24,734	26,617	17,702	38,768	55,874	53,722	476,166	482,448	468,686
NaN_3	0	47,427	27,816	33,822	22,037	25,574	26,509	47,879	71,128	86,779
NaN_3	1	17,056	15,590	28,737	47,687	30,921	55,460	58,618	52,801	75,276
NaN_3	10	48,985	26,189	39,286	41,011	44,837	41,481	99,199	137,922	128,720
NaN_3	100	41,150	60,360	31,422	36,764	62,417	61,596	459,433	473,881	427,359
catalase	0	47,781	25,839	97,988	24,872	37,852	55,740	24,774	36,194	57,786
catalase	1	32,277	18,911	88,941	25,228	47,957	62,449	34,302	31,904	54,776
catalase	10	30,189	24,960	82,044	31,421	39,031	88,171	39,161	54,221	66,499
catalase	100	27,512	34,883	69,835	25,678	32,090	94,073	103,725	102,097	137,047

Table S6. Raw fluorescence values for determining selectivity of **1**: Reaction with $^1O_2$. Data shown are the fluorescence at 40 min minus the fluorescence at 0 min. *n* = 3.

Determining selectivity of 1: Reaction with •OH

•OH was generated through the reaction of $FeSO_4$•$7H_2O$ with H_2O_2. A solution of 100 μM **1** in ethanol (20 μL) was added to 5:95 methanol/50 mM phosphate pH 7 buffer (140 μL). Water or 10^4 U/mL catalase (20 μL) was added to the mixture. $FeSO_4$•$7H_2O$ (27.4 mg) was added to ultrapure water (2.00 mL). This solution was diluted to 20 μM, 200 μM, and 2.00 mM. H_2O_2 was diluted to 200 μM and 2.00 mM. Equal volumes of $FeSO_4$•$7H_2O$ solution and H_2O_2 were added together, and an aliquot (20 μL) was immediately transferred to the solution containing **1**. The fluorescence intensity was measured immediately and again after incubation at 25 ˚C for 40 min.

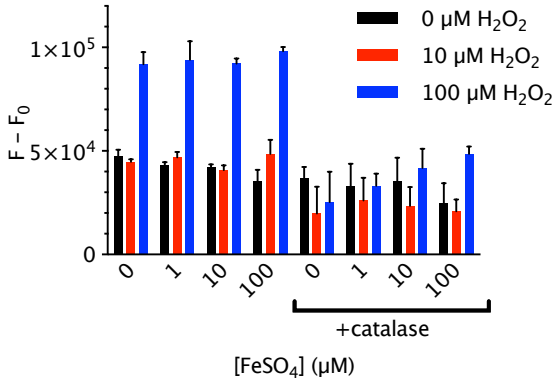

Figure S9. Determining selectivity of **1**: Reaction with •OH.

Additive	[$FeSO_4$] (μM)	0 μM H_2O_2			10 μM H_2O_2			100 μM H_2O_2		
	0	50,173	48,124	44,143	43,929	46,186	43,989	94,742	95,713	85,271
	1	44,775	42,847	41,775	49,425	47,262	44,251	103,905	91,684	86,594
	10	43,299	42,365	40,214	42,933	40,908	38,283	90,712	94,948	91,049
	100	32,709	41,651	31,615	56,260	46,281	43,358	99,391	95,778	99,384
catalase	0	31,506	41,640	38,159	16,840	33,959	8,517	37,819	28,926	9,145
catalase	1	28,688	24,659	45,310	31,319	13,633	33,399	34,591	26,790	38,285
catalase	10	24,822	33,920	47,376	19,991	16,693	33,776	42,724	50,635	32,300
catalase	100	35,828	18,194	20,321	20,486	26,765	15,423	46,921	52,666	46,232

Table S7. Raw fluorescence values for determining selectivity of **1**: Reaction with •OH. Data shown are the fluorescence at 40 min minus the fluorescence at 0 min. *n* = 3.

Determining selectivity of 1: Reaction with ClO^- and $ONOO^-$

A solution of 0, 1, 10, or 22 μM $ONOO^-$ in 0.3 M NaOH (20 μL) or 1, 10, 100, or 1000 μM NaOCl in water (20 μL) was added to the wells of a black 96-well plate. A solution of 10 μM 1 in DMSO (560 μL) and 5:95 MeCN/1.2 M phosphate pH 7 buffer (4.48 mL) was made; this solution (180 μL) was transferred to each of the wells. The samples were allowed to incubate at 25 °C for 15 min before the fluorescence was measured.

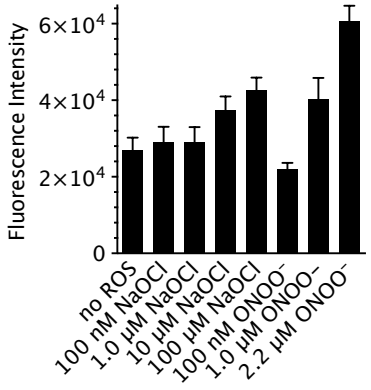

Figure S10. Determining selectivity of **1**: Reaction with ClO^- and $ONOO^-$.

	Fluorescence Intensity		
no ROS	30,591	24,478	26,025
100 nM NaOCl	33,503	25,413	28,088
1.0 μM NaOCl	28,551	25,590	33,211
10 μM NaOCl	41,611	35,271	35,308
100 μM NaOCl	46,362	40,070	41,695
100 nM $ONOO^-$	23,606	21,961	20,229
1.0 μM $ONOO^-$	46,271	39,358	35,209
2.2 μM $ONOO^-$	63,954	56,351	61,987

Table S8. Raw fluorescence values for determining selectivity of **1**: Reaction with ClO^- and $ONOO^-$. *n = 3.*

Determining selectivity of 1: Reaction with ^{t}BuOOH

A solution of 5:95 MeCN/50 mM phosphate pH 7 buffer (160 μL) was added to the wells of a black 96-well plate. 10 μM **1** in DMSO (20 μL) was added to each well. 0 mM H_2O_2 in water (20 μL) or 0, 10, or 100 μM ^{t}BuOOH in DMSO (20 μL) were then added to the wells. The samples were allowed to incubate at 25 °C for 15 min before the fluorescence was measured.

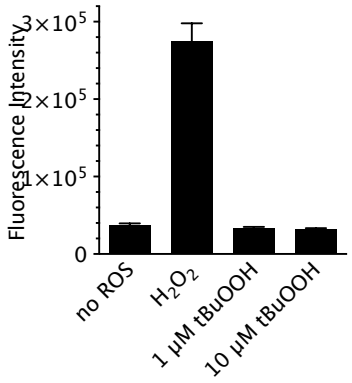

Figure S11. Determining selectivity of **1**: Reaction with ^{t}BuOOH

	Fluorescence Intensity		
no ROS	34,525	36,401	39,836
H_2O_2	277,013	296,506	250,145
1 μM ^{t}BuOOH	32,951	29634	34,860
10 μM ^{t}BuOOH	31,650	28,922	33,363

Table S9. Raw fluorescence values for Determining selectivity of 1: Reaction with ^{t}BuOOH. *n* = 3.

Determining selectivity of 1: Reaction with NO_2^-

$NaNO_2$ (97.0 mg) was dissolved in ultrapure water (2.00 mL). This solution was diluted to 10 μM, 100 μM, 1.00 mM, and 10.0 mM. H_2O_2 was diluted to 10 μM, 100 μM, 1.00 mM, and 10.0 mM. A solution of 100 μM **1** in ethanol (20 μL) was added to 5:95 methanol/50 mM phosphate pH 7 buffer (160 μL). The $NaNO_2$ or H_2O_2 solutions (20 μL) were added to the solution containing **1** and the fluorescence intensity was measured immediately and again after incubation at 25 ˚C for 15 min.

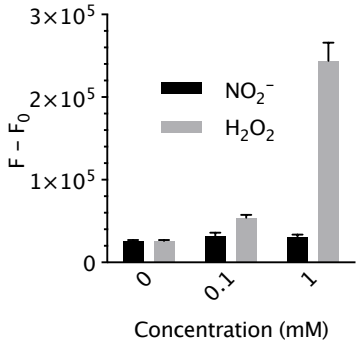

Figure S12. Determining selectivity of **1**: Reaction with NO_2^-. *n* = 3.

[NO_2^-] or [H_2O_2] (μM)	NO_2^-			H_2O_2		
0	24,359	26,870	26,226			
0.1	31,075	36,429	27,504	58,172	52,104	52,249
1	26,768	31,470	33,004	266,770	242,313	222,834

Table S10. Raw fluorescence values for determining selectivity of **1**: Reaction with NO_2^-. Data shown are the fluorescence at 15 min minus the fluorescence at 0 min. *n* = 3.

Determining selectivity of 1: Reaction with NO_3^-

$NaNO_3$ (30.9 mg) was dissolved in ultrapure water (2.00 mL). This solution was diluted to 10 μM, 100 μM, 1.00 mM, and 10.0 mM. H_2O_2 was diluted to 10 μM, 100 μM, 1.00 mM, and 10.0 mM. A solution of 100 μM **1** in ethanol (20 μL) was added to 5:95 methanol/50 mM pH 7 potassium phosphate buffer (160 μL). The $NaNO_3$ or H_2O_2 solutions (20 μL) were added to the solution containing **1** and the fluorescence intensity was measured immediately and again after incubation at 25 ˚C for 15 min.

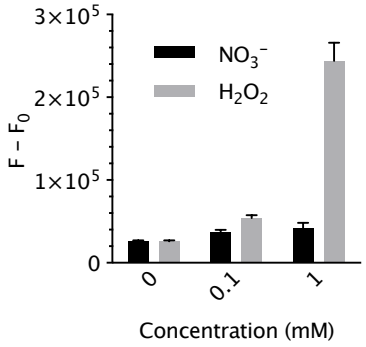

Figure S13. Determining selectivity of **1**: Reaction with NO_3^-. *n* = 3.

[NO_3^-] or [H_2O_2] (μM)	NO_3^-			H_2O_2		
0	24,359	26,870	26,226			
0.1	34,507	35,439	40,487	58,172	52,104	52,249
1	43,966	35,385	47,433	266,770	242,313	222,834

Table S11. Raw fluorescence values for determining selectivity of **1**: Reaction with NO_3^-. Data shown are the fluorescence at 15 min minus the fluorescence at 0 min. *n* = 3.

Determining selectivity of 1: Reaction with NO•

A NO• solution was generated by the addition of H_2SO_4 to $NaNO_2$. A round-bottom flask containing a saturated solution of $NaNO_2$ was connected to a series of three bubblers and one Erlenmeyer flask; the first two bubblers contained 30% NaOH, and the third contained ultrapure water. The flask contained ultrapure water (10 mL). The solutions were degassed with argon for 30 min. Then a 2 M solution of H_2SO_4 (1 mL) was added to the saturated $NaNO_2$ to produce a 1.8 mM solution of NO• (assuming saturation at 25 °C) in the flask. A solution of 10 μM **1** in DMSO (20 μL) was added to 5:95 acetonitrile/50 mM pH 7 potassium phosphate buffer (160 μL). The NO• solution (20 μL) was then added to the mixture containing **1**. The fluorescence was measured immediately and again after 15 min at 25 °C.

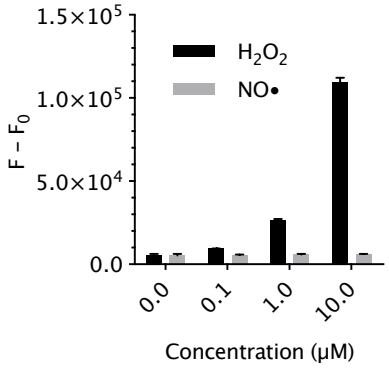

Figure S14. Determining selectivity of **1**: Reaction with NO•. *n* = 3.

[NO•] or [H_2O_2] (μM)	NO•			H_2O_2		
0	4,567	5,018	6,300			
0.1	5,344	5,827	5,393	9,370	9,525	9,517
1	6,268	5,961	5,430	26,155	26,618	27,176
10	6,104	6,207	5,735	111,008	106,765	111,053

Table S12. Raw fluorescence values for Determining selectivity of **1**: Reaction with NO•. Data shown are the fluorescence at 15 min minus the fluorescence at 0 min. *n* = 3.

pH dependence of the reaction of 1 with H_2O_2

A solution of 50 mM phosphate pH 7.3 buffer was treated with 1.0 N HCl to adjust the pH to 7.0, 6.5, 5.9, 5.4, 4.5, or 4.1. The concentration of the resulting buffers was adjusted with water to 25 mM phosphate buffer. Solutions of 25 mM phosphate pH 7.3, 7.0, 6.5, 5.9, 5.4, 4.5, or 4.1 buffer (160 µL) and 100 µM probe **1** in MeOH were treated with 100 µM, 10 µM or 0 µM H_2O_2 in water. The solutions were allowed to incubate at 23 ºC for 20 min prior to measuring the fluorescence.

pH	10 µM H_2O_2			1 µM H_2O_2			0 µM H_2O_2		
7.30	372,555	388,584	401,912	228,368	208,913	186,665	189,898	183,424	169,054
7.00	389,464	369,467	390,006	247,464	221,499	229,530	199,101	207,136	187,676
6.50	332,896	341,948	335,544	203,661	188,050	184,986	155,151	183,747	149,421
5.90	167,836	187,633	154,515	113,703	111,368	107,545	87,499	89,708	90,424
5.40	103,516	107,311	103,354	61,365	63,294	60,943	56,192	56,334	52,671
4.50	55,577	54,961	56,315	40,599	31,790	33,283	29,770	29,064	29,069
4.10	51,632	54,097	52,472	35,884	30,492	30,471	28,470	29,037	28,661

Table S13. Raw fluorescence intensities for the reaction of **1** with H_2O_2 at pH 4.1–7.3.

pH dependence of phenol 5

Phenol **5** was dissolved in water to a concentration of 100 nM. This solution (100 mL) was titrated with HCl and NaOH. The pH was measured after each addition before measuring the fluorescence using a Horiba FluoroMax3 fluorescence spectrometer. Fluorescence was measured using 1 nm slit widths with an excitation wavelength of 496 nm and an emission wavelength of 510 nm.

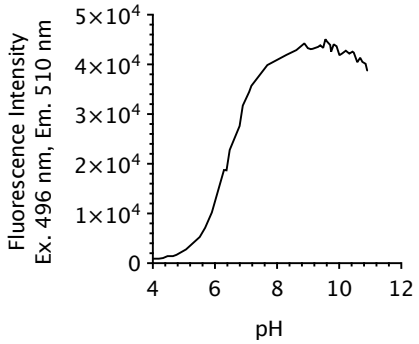

Figure S15. The pH dependence of phenol **5**.

pH	Fluorescence Intensity
3.99	920
4.20	930
4.33	1,070
4.48	1,450
4.65	1,440
4.77	1,670
5.07	2,790
5.51	5,280
5.69	7,130
5.90	10,250
6.30	18,790
6.38	18,720
6.48	22,820
6.80	27,620
6.90	31,730
7.11	34,510
7.18	35,740
7.69	39,880
8.31	41,950
8.63	42,930
8.88	44,240
9.00	43,280
9.09	43,110
9.15	43,140
9.32	43,550
9.40	43,850
9.49	43,340
9.56	45,080
9.61	44,640
9.71	43,930
9.75	42,610
9.83	44,070
9.92	43,670
10.01	41,900
10.10	42,170
10.22	42,800
10.33	42,170
10.43	42,570
10.48	42,410
10.59	40,450
10.68	41,370
10.75	40,520
10.85	40,140
10.91	38,790

Table S14. Raw fluorescence values for the pH dependence of hydroxymethyl Tokyo Green.

Cellular Imaging

Cells were seeded on 35-mm glass bottom dishes (MatTek Corporation, Ashland, MA) and incubated with 0.5 μM **1** in 0.1% DMSO in DMEM (10% FBS with penicillin/streptomycin) for 15 min prior to imaging. In some cases, cells were incubated with 1 μM MitoTracker® Red FM (ThermoFisher Scientific) for 20 min at 37 °C. The treated cells were washed with HBSS, and the media was replaced with HBSS (2.00 mL). The dish was inserted in a closed, thermo-controlled (37 ºC) stage top incubator (Tokai Hit Co., Shizuoka-ken, Japan) atop the motorized stage of an inverted Nikon TiE fluorescent microscope (Nikon Inc., Melville, NY) equipped with a 60X oil immersion optic (Nikon, CFI PlanFluor, NA 1.49) and NIS Elements Software. The sample was excited using the 470 nm line of a Lumencor diode-pumped light engine (SpectraX, Lumencor Inc., Beaverton OR). Fluorescence was detected using an ET-GFP filter set (Chroma Technology Corp) and ORCA-Flash 4.0 sCMOS camera (HAMAMATSU Corporation, Bridgewater, NJ). MitoTracker Red was excited using the 555 nm line and detected using a TRITC filter set. Data were collected every 30 s over a 10-min period.

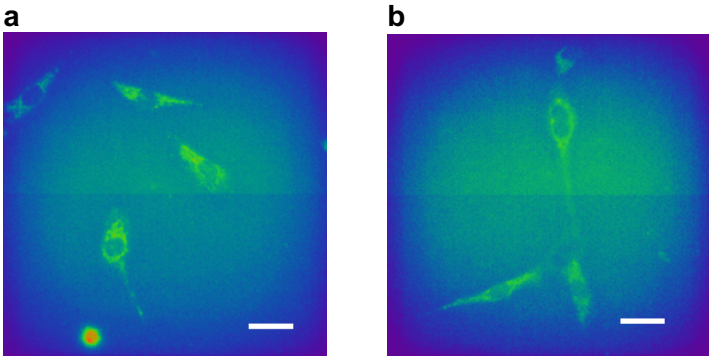

Figure S16. Pseudo-color image of RAW cells loaded with 5 μM dihydrodichorofluorescein diacetate. (a) Without stimulation by ionomycin. (b) With stimulation by ionomycin. The scale bars are 20 μm.

Zebrafish tail-wounding model

Three-day post-fertilization zebrafish embryos were removed from their chorion and allowed to swim in 1 mM **1** for 2 h (0.1% v/v DMSO), leading to effective dye loading. Following this, the fish were anesthetized and mounted in agar. The tail fins were clipped with a razor blade. Fluorescence images were obtained every 60 s for 60 min using an inverted Nikon TiE fluorescent microscope (Nikon Inc., Melville, NY) equipped with a 20X 0.75 NA lens and NIS Elements Software. The sample was excited using the 470 nm line of a Lumencor diode-pumped light engine (SpectraX, Lumencor Inc., Beaverton OR), and the fluorescence signals were detected using an ET-GFP filter set (Chroma Technology Corp) and ORCA-Flash 4.0 sCMOS camera (HAMAMATSU Corporation, Bridgewater, NJ).

References

1. L. Ying; B. P. Bruce; *Bioconj. Chem.*, **2011**, *22*, 987–992.
2. S. Ando, K. Koide; *J. Am. Chem. Soc*. **2011**, *133*, 2556–2566.
3. A. Krief, F. Lonez; *Tetrahedron Lett.* **2002**, *35*, 6255–6257.

Author Contributions

K.K. conceived the project and designed the probe. U.B. and I.P. synthesized the probe (Figure 2). I. P. performed the mechanistic studies (Figure 3) and pH dependence study (Figure 5c). U. B. performed kinetic studies (Figure 4). D.P. performed the experiments described in Figure 5a and Figure 5b. D.P., C.M.C., and S.C.W. performed the experiments described in Figures 6 and 7. D.P., I.P., and K.K. wrote the manuscript.

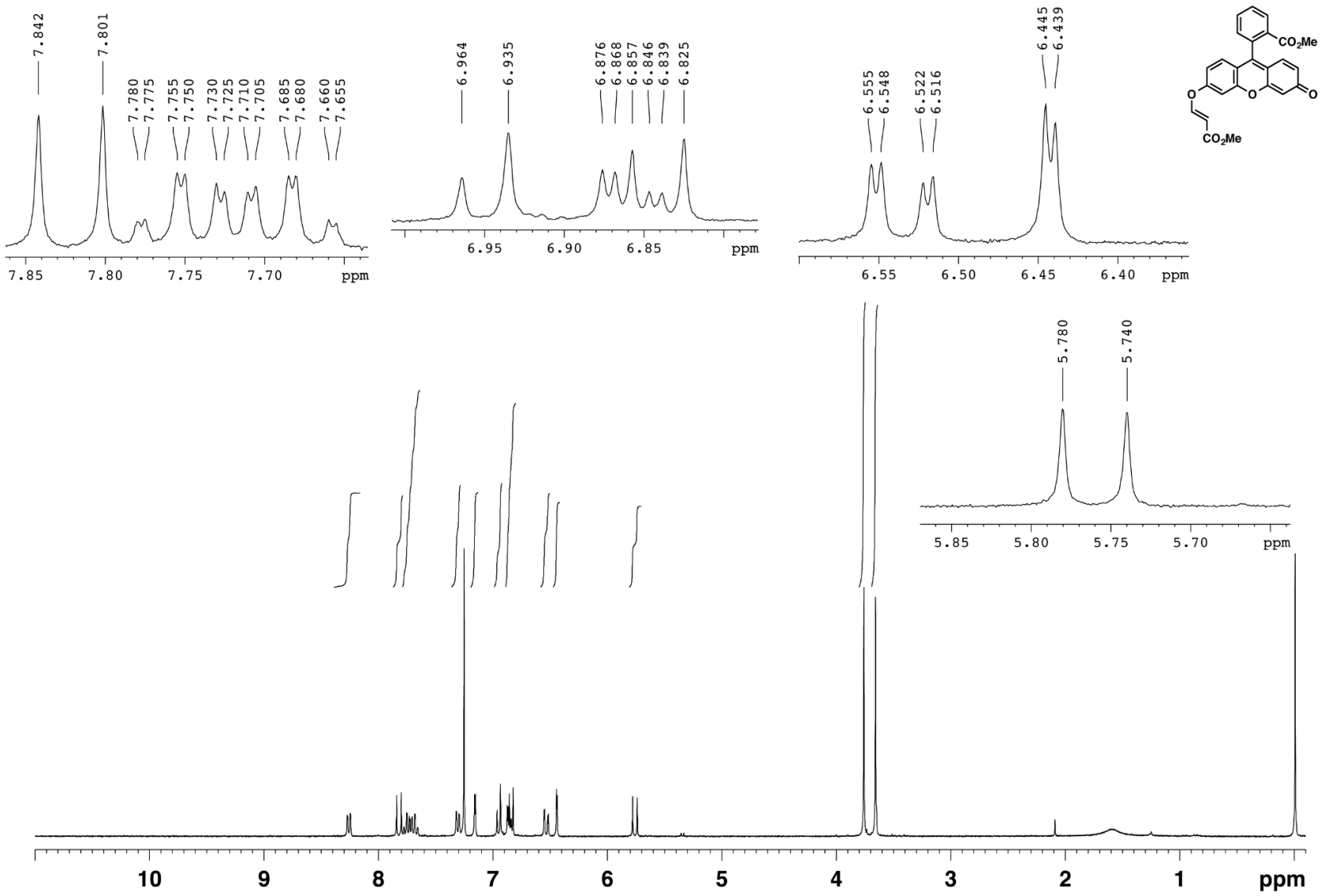

Spectrum 1. ^{1}H NMR spectrum of **8** (300 MHz, $CDCl_3$, 293K).

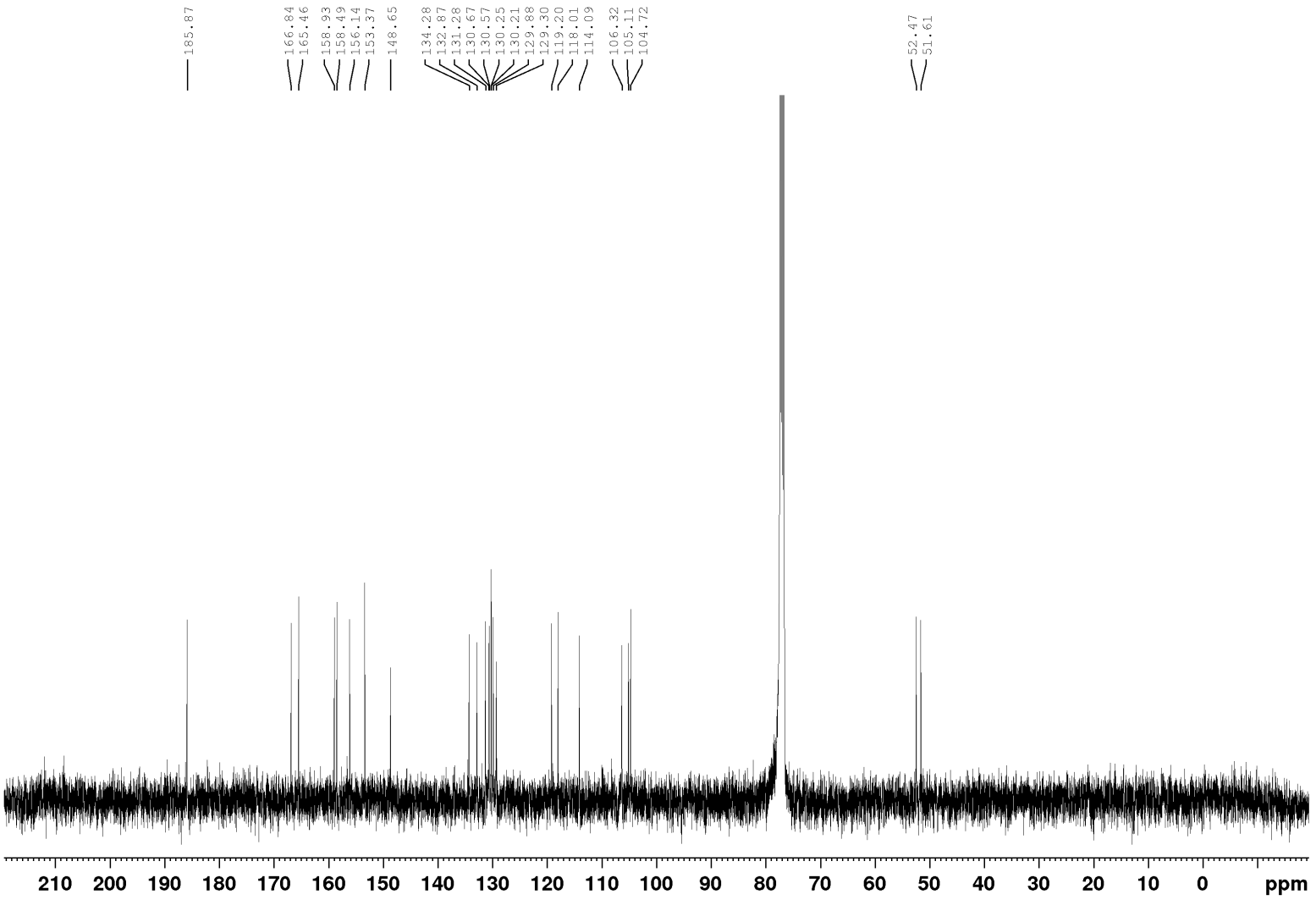

Spectrum 2. ^{13}C NMR spectrum of **8** (100 MHz, $CDCl_3$, 293K).

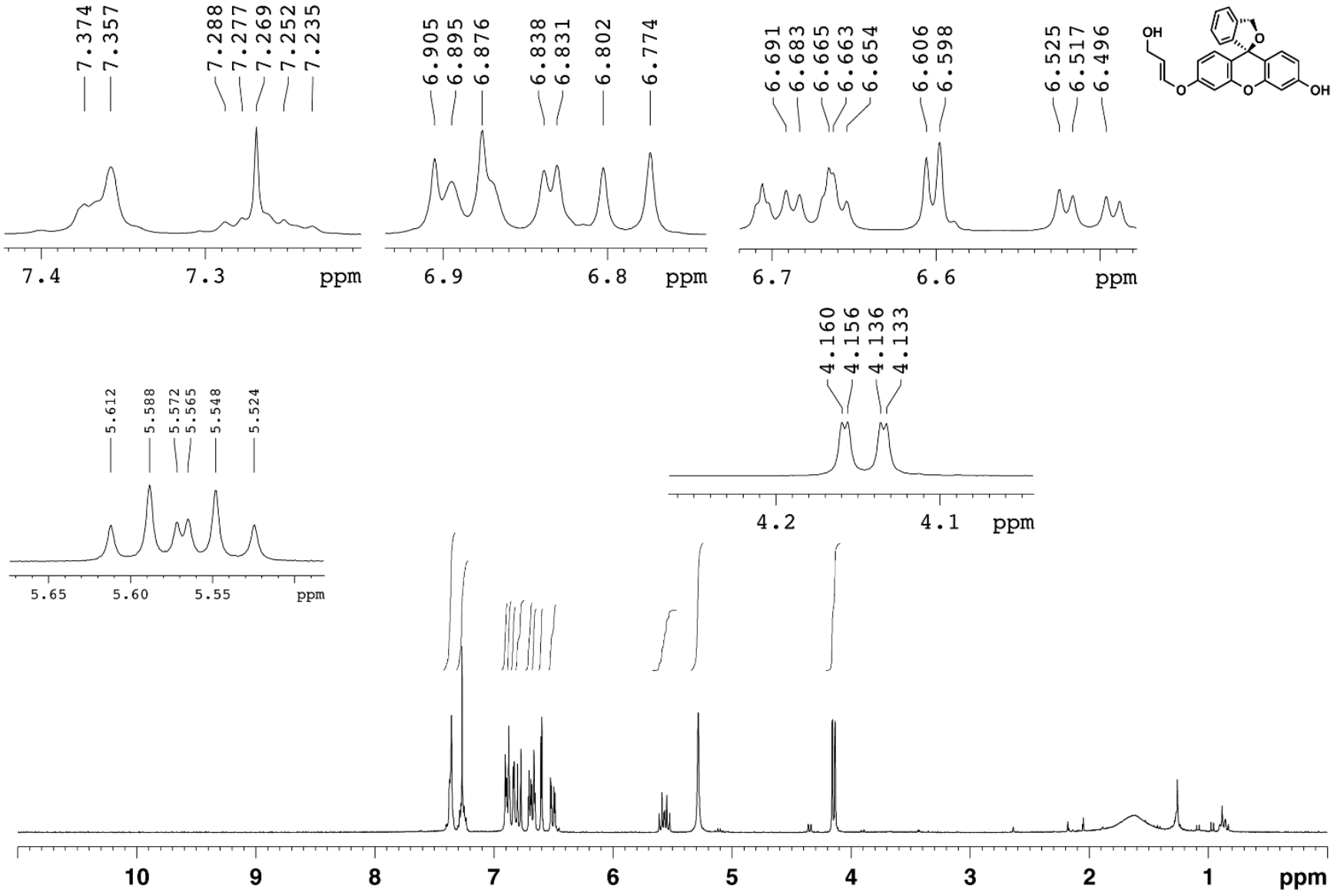

Spectrum 3. ^{1}H NMR spectrum of **9** (300 MHz, $CDCl_3$, 293K).

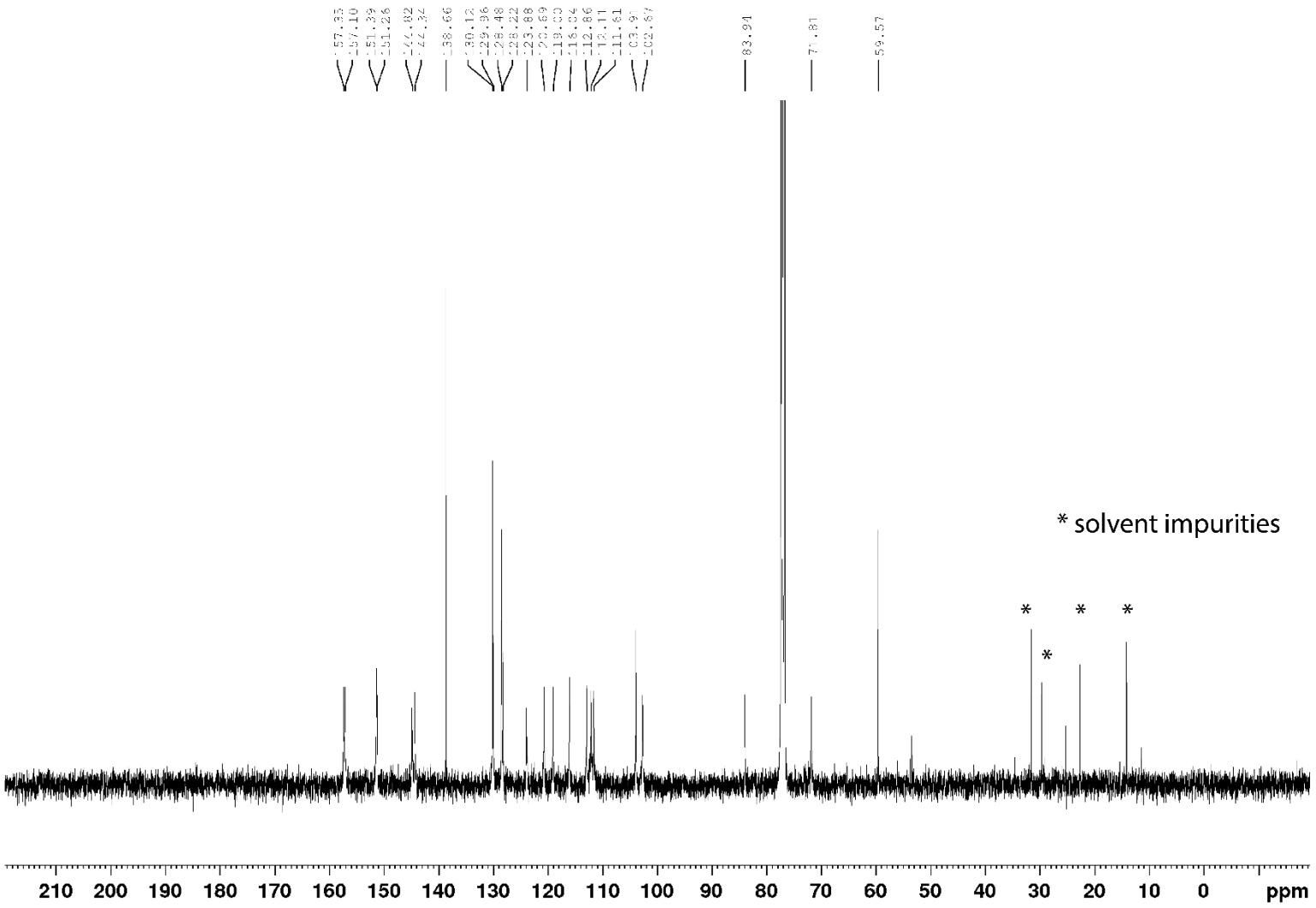

Spectrum 4. ^{13}C NMR spectrum of **9** (100 MHz, $CDCl_3$, 293K).

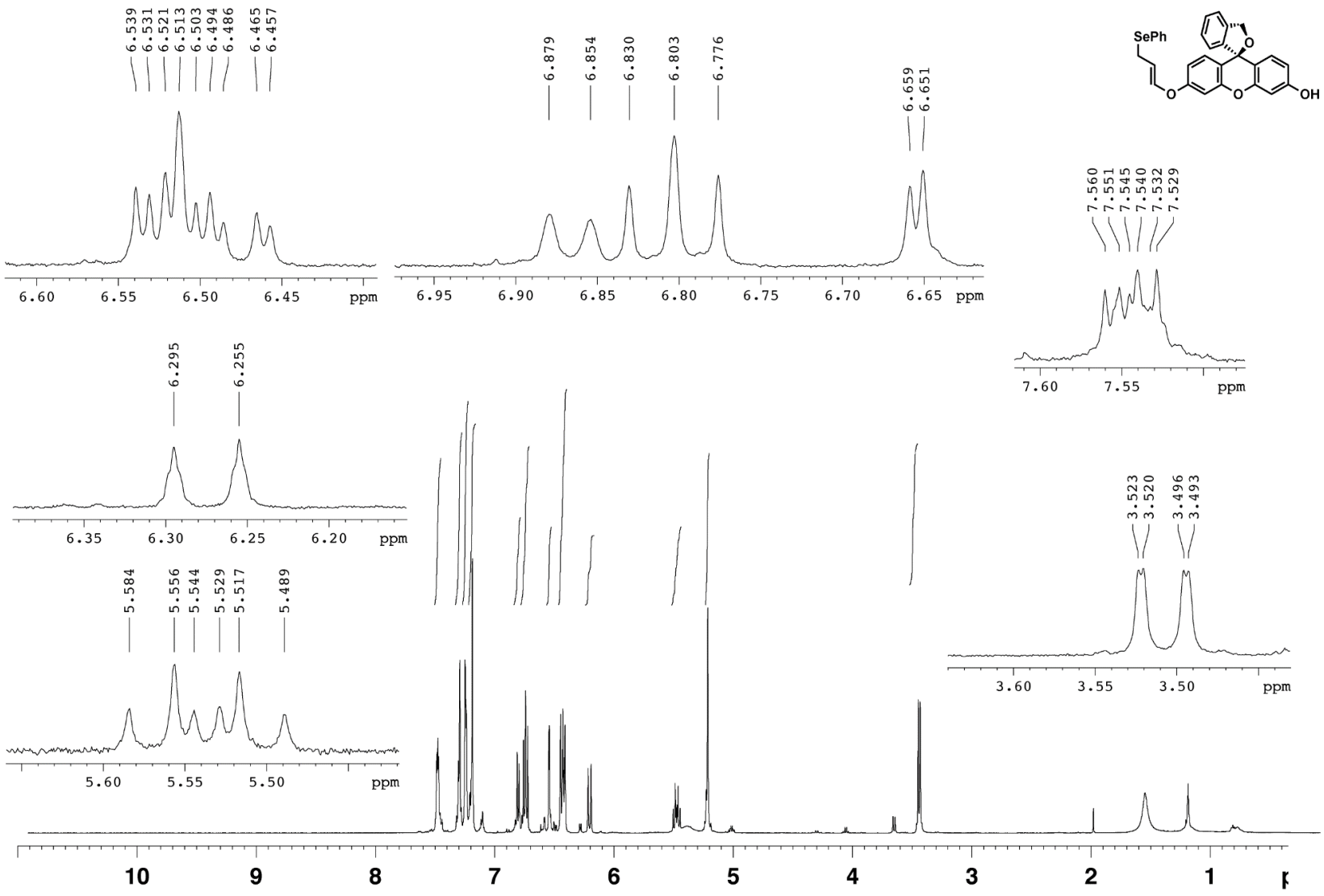

Spectrum 5. ^{1}H NMR spectrum of **1** (300 MHz, $CDCl_3$, 293K).

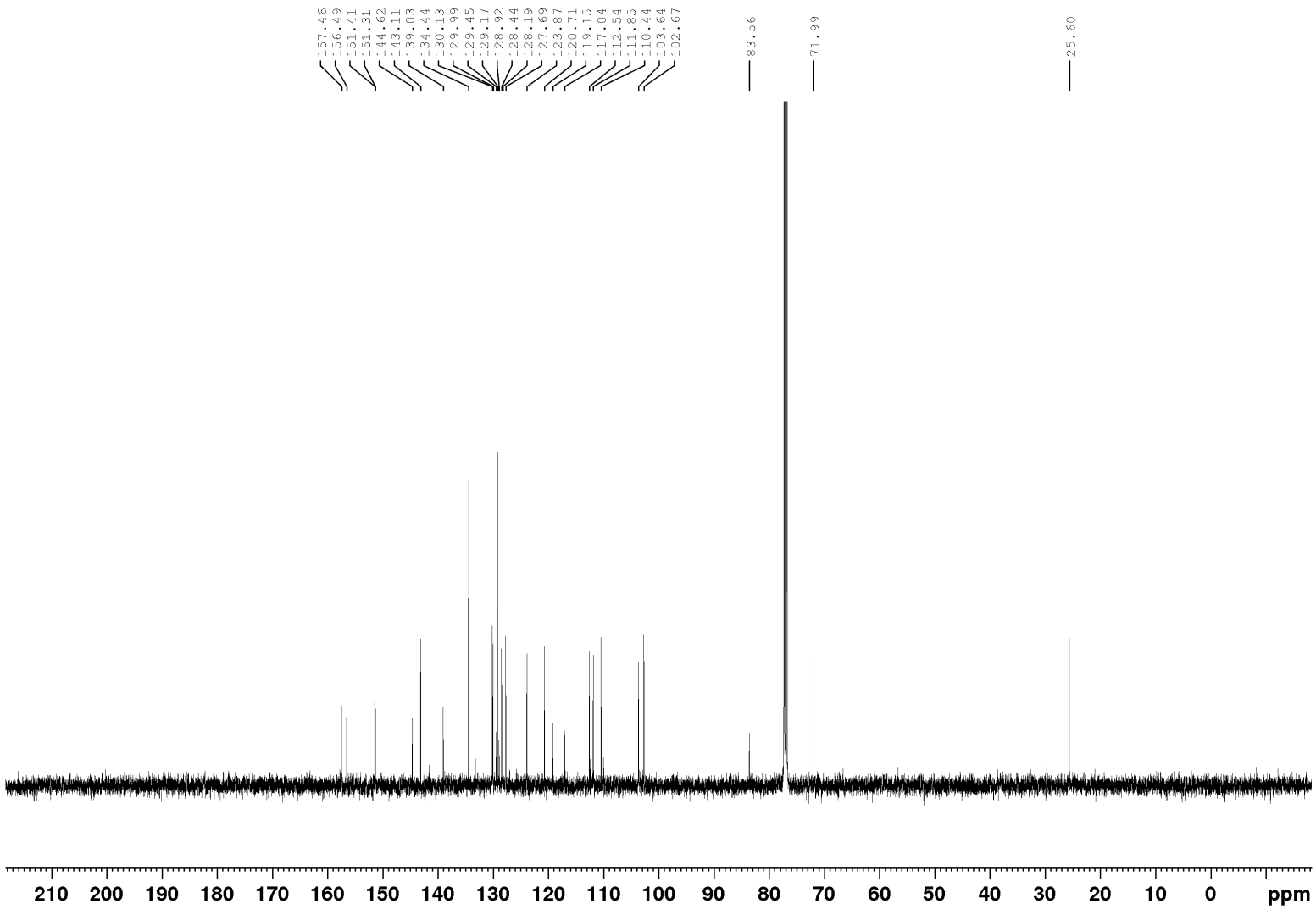

Spectrum 6. ^{13}C NMR spectrum of **1** (100 MHz, $CDCl_3$, 293K).